

NASA Technical Memorandum 86751

1N-05

72552

DATE OVERRIDE

P-70

(NASA-TM-86751) ANALYSIS OF THE FREE-TIP
ROTOR WIND-TUNNEL TEST RESULTS (NASA) 70 p
Avail: NTIS HC AC4/MF A01 CACL 01C

N87-21915

Unclas
H1/05 0072552

Analysis of the Free-Tip Rotor Wind-Tunnel Test Results

Robert H. Stroub

May 1985



National Aeronautics and
Space Administration

Date for general release May 1987

Analysis of the Free-Tip Rotor Wind-Tunnel Test Results

Robert H. Stroub, Ames Research Center, Moffett Field, California

May 1985



National Aeronautics and
Space Administration

Ames Research Center
Moffett Field, California 94035

SYMBOLS

A_{1c}	lateral cyclic control, deg
A_O, A_N, B_N	coefficients of Fourier equation
a	$\left[\omega^2 + \left(\frac{\Delta \dot{\theta}_O}{I \Delta \theta_O} \right)^2 \right]^{1/2}$
a.c.	aerodynamic center
B_{1s}	longitudinal cyclic control, deg
b	span of free tip, m
b_A	aerodynamic damping moment, N·m sec/rad
b_f	friction damping moment, N·m
C_1	lift deficiency factor
C_{D_t}	tip drag coefficient, $\frac{\text{drag}}{0.5 \rho S_t V^2}$
C_{L_t}	tip lift coefficient, $\frac{\text{lift}}{0.5 \rho S_t V^2}$
C_{L_α}	rate of change of lift with angle of attack, deg ⁻¹
C_L / σ	rotor lift coefficient, $\frac{\text{rotor lift}}{\rho S (\Omega R)^2}$
C_{m_t}	tip pitching moment coefficient, positive nose-up, $\frac{\text{pitching moment}}{0.5 \rho S_t c_t V^2}$
C_{m_α}	rate of change of tip pitching moment with angle of attack, positive nose-up, deg ⁻¹
C_p / σ	rotor power coefficient, $\frac{(\text{torque}) \Omega}{\rho S (\Omega R)^3}$
c	blade chord, m

c.g.	center of gravity
c_t	reference chord of tip, m
$dM_{sp}/d\phi$	rate of change of torsional moment with elastic twist of tension torsion strap, N·m/deg
F_{CF}	centrifugal force, N
I	moment of inertia of the tip about the pitch axis, $kg \cdot m^2$
i_t	incidence angle, deg
K_α	equivalent aerodynamic spring constant, $0.5C_{m_\alpha} \rho S_t c_t V^2$, N·m/rad
k	spring constant of controller, N·m/rad
l	length of the untwisted torsion straps, m
M_c	control moment, N·m
M_β	pitching moment induced by flapping, N·m
M_ζ	pitching moment induced by lead-lag, N·m
m	mass of tip, kg
R	rotor radius, m
r	radius from pitch axis centerline, m
r_b	radial distance from rotor hub centerline to measurement station, m
rpm	revolutions per minute
S	planform area of rotor blades, m^2
S_t	tip planform area, m^2
S_w	wing planform area, m^2
T	period of one cycle, sec
TR	inertial feathering moment with pitch angle, N·m/rad
V	free-stream velocity, m/sec
\bar{X}	rotor propulsive force coefficient, $-\text{drag}/2\rho V^2 S/\pi$

α_t	angle of attack of tip, deg
α_w	wing angle-of-attack, deg
β	blade flapping angle, deg
$\dot{\beta}, \ddot{\beta}$	first and second time-derivative of blade flap angle, rad/sec, rad/sec ² , respectively
Δc	pitch axis and aerodynamic center offset, m
$\Delta\alpha$	angle-of-attack change, deg
$\Delta\theta$	tip pitch angle relative to the inboard portion of blade, positive nose-up, deg
$\Delta\dot{\theta}, \Delta\ddot{\theta}$	first and second time-derivative of $\Delta\theta$, rad/sec, rad/sec ² , respectively
ζ	blade lead-lag angle, deg
$\dot{\zeta}, \ddot{\zeta}$	first and second time-derivative of blade lead-lag angle, rad/sec, rad/sec ² , respectively
θ_c	total pitch angle of tension-torsion strap, deg
θ_λ	pitch angle of inboard portion of blade relative to rotor-disk plane, deg
θ_t	tip pitch angle relative to rotor-disk plane, deg
$\theta_{0.75}$	pitch angle at 0.75 R, deg
Λ	sweep angle, deg
λ	exponential decay coefficient, sec ⁻¹
ρ	density of air, kg/m ³
ϕ	strap helical angle, deg
ψ	azimuth angle, deg
ΩR	tip speed, m/sec
ω	damped natural frequency, rad/sec

SUMMARY

The results from a wind-tunnel test of a small-scale free-tip rotor are analyzed. The free-tip rotor has blade tips that are free to weathervane into the tip's relative wind, thus producing a more uniform lift around the azimuth. The free tip extended over the outer 10% of the rotor blade and included a simple, passive controller mechanism. The free-tip assembly, which includes the controller, functioned flawlessly throughout the test. In a test of the free-tip's response after passing through a vertical air jet, the tip pitched freely and in a controlled manner. Analysis of the tip's response characteristics showed the free-tip system's damped natural frequency to be 5.2 per rev. Tip pitch-angle responses to the local airstream are presented for an advance-ratio range of 0.1 to 0.397 and for a solidity weighted rotor lift-coefficient range of 0.038 to 0.092. Harmonic analysis of the responses showed a dominance by the first harmonic. Only at low advance ratios were there significant contributions from the higher harmonics. As a result of the tip being free, forward flight power requirements were reduced by 8% or more. Considerably more power reduction was recorded for high-thrust conditions. The reduction in power requirements was attributed to a favorable influence of the tip's negative pitch angle relative to the inboard portion of the blade; a hypothesis is presented to account for that favorable effect. The lessening of tip drag because of its negative relative pitch angle was also supported by fixed-wing wind-tunnel test of the same tip shape. In addition to the power reduction, flatwise blade bending moments were reduced by as much as 30% at the inboard blade stations. Chordwise loads, however, were not reduced by the free tip. Loads going into the control system were reduced at all speeds and rotor lift levels. Details of tip and controller design and construction are included.

INTRODUCTION

It is a major objective of helicopter research to develop means of improving performance and reducing vibration. Since performance and vibration can be affected by the blade tip, the tip has been the subject of considerable study. The free tip is one of the proposed design changes, and it holds considerable promise for improving performance and lessening oscillatory loads and vibration.

The free tip (fig. 1) is characterized by (1) being separated from the rest of the blade, (2) by having the pitch axis forward of the aerodynamic center, and (3) by a control moment that is applied about the pitch axis. These characteristics add a new pitch degree of freedom to the tip's motion. With the added pitch degree

of freedom, the tip weathervanes into its relative wind to produce a moment balance about the pitch axis. The tip weathervanes about a prescribed null point that results in a finite pitch moment and, consequently, in a finite lift. Therefore, the free tip may generate a lift level that is nearly constant as it goes around the azimuth.

The free-tip design was derived as an offshoot from the constant-lift rotor described in reference 1. The constant-lift rotor had many free pitching segments along the blade radius, and it included a pilot-controlled mechanism to vary the lift both collectively and cyclically. For the free-tip design, only one free pitching segment was included and there was no mechanism to vary the lift either collectively or cyclically by the pilot.

An analytical investigation of the free-tip was carried out to quantify a potential gain in rotor forward flight performance (ref. 2). That investigation concluded that a 10% reduction in power could be realized if the free tip would eliminate the negative lift on the advancing tip.

Although the free tip seemed attractive on a performance-improvement basis, there was considerable concern about the practicality of building it. Could the tip mass be balanced about the pitch axis at the 0.125 chord line? Could the polar moment of inertia be low enough to allow reasonable dynamic response? Could a simple controller be built? These questions were addressed under a contracted preliminary design study (ref. 3). It was concluded that a tip could be mass-balanced about the 0.125 chord line, with a resulting moment of inertia that would enable an undamped natural frequency of 7 to 8 per rev, based on its aerodynamic spring rate; moreover, a simple controller could be easily built.

Given the high performance-improvement potential and the feasibility of constructing the tip and controller, an investigation was undertaken to explore experimentally the result of having a free tip on a rotor blade. A small-scale model rotor was modified to accept the first free tip. The rotor blade was modified by installing a steel pitch shaft at 13% chord to carry the free tip. A helical groove, cut into the steel shaft, accepted a guide pin which was inserted through the leading edge of the free tip and held in place by a retaining screw. This arrangement allowed the tip to pivot freely within the limits of the groove and still remain secured on the shaft. In addition, this arrangement causes the guide pin to carry the full centrifugal-force loading with the potential of having very high friction between the pin and the groove. To minimize friction, the guide pin and groove were lubricated by an oven-bonded dry lubricant. The pin in the helical groove was the tip's radial restraint and also served as the "controller," the device which produces a pitching moment about the pitching axis. The pin in the helical groove produced the pitching moment by creating a component of the tip's centrifugal load parallel to the helical groove in the shaft. Because this force component was acting at a radial distance from the centerline of the shaft, a torque was produced.

The model was built, bench tested, and then tested in the wind tunnel. In the wind-tunnel test, the tip did not pitch freely. In fact, it hardly pitched at

all. The tip went to a nominal pitch angle that was 10° greater than the inboard portion of the blade and oscillated only $\pm 0.5^\circ$ around the nominal setting. The tip's motion was limited, even though the advancing-tip Mach number was as much as 0.83. The test results were reported in references 4 and 5.

Post-test analysis revealed a number of shortcomings in this design. First, the 0.05 R span of the free tip was too short, which made it impossible to utilize the lifting potential of inboard stations to increase the weathervaning capability. Second, the centrifugal force of the tip was carried across surfaces in sliding contact, which increased the tip's susceptibility to high friction losses that inhibited motion. Third, the controller was designed so the control moment could not be adjusted from the design value. This made it impossible to evaluate the design over a broad range of tip aerodynamic loading.

Since this first wind-tunnel test demonstrated design shortcomings of the model rotor tested but not of the free-tip idea, a new free-tip evaluation program was commenced. In that program, several potential controllers and tip shapes were considered and tested. The best controller and the best tip shape were then incorporated into a model rotor which was tested in the Boeing Vertol wind tunnel.

The purpose of this report is to present the analysis and results of the first successful free-tip wind-tunnel test. Also presented are the results of developmental tests of the free-tip system that preceded the wind-tunnel tests. A complete set of data from the wind-tunnel test is presented in reference 6.

MODEL DESCRIPTION

An existing four-bladed, 5.09-m-diam, Mach-scaled model rotor was modified to incorporate the free-tip design. The complete rotor with the free tip is shown in figure 2; figure 3 shows a close-up of the tips. This rotor was modified by installing a steel pitch shaft at the tip on the 13% chord line. The shaft transferred tip bending and shear loads to the inboard portion of the blade; it also served as the pitch axis about which the tip was free to oscillate.

The pitch shaft was hollow to allow a concentric inner shaft to grip the free tip and extend into the inboard portion of the blades where it attached to the controller mechanism. The inner shaft served to retain the tip against centrifugal force and to transmit the pitch-control moment. Figure 4 shows the total configuration. The tip is retained, using a locknut arrangement in which the "nut" is an integral part of the free tip and is clamped to the threaded end of the shaft. A Rulan bearing applied to the shaft minimized the frictional forces between the free tip and the pitch shaft.

The controller mechanism is a simple wire-wound, tension-torsion strap. A continuous high-strength wire, 0.152 mm diam, was wrapped 275 times around two spools placed 5.71 cm apart. One spool was fixed to the inboard portion of the blade and the other spool was attached to the inboard end of the inner shaft with a

clevis joint. The straps were encased in an elastomer material which kept the straps separated when subjected to angular deflections greater than 90°. Without the elastomer between the straps, the straps would come together, and the output torque would decrease to an unacceptably low value. Large angular pitch deflections between the two spools were an integral part of the design criteria. The straps were fatigue-tested to over 2 million cycles of $\pm 10^\circ$ pitch changes while carrying the full design tension load and pretwisted to 125°.

The controller carries the tip's full centrifugal force and uses it to produce most of the desired control moment. Control moment is produced by the centrifugal force acting on the torsionally twisted straps as indicated in figure 5. An additional control moment component was the mechanical bending of wires and twisting of elastomer that accompanied twisting the straps. The total torsional moment is computed by

$$M_c = rF_{CF} \tan \phi + [dM_{sp}/d\phi]\phi \quad (1)$$

Although this equation reflects the proper physical relationship, the torsional twist angle term ϕ is not convenient to use. A more convenient term is θ_c , the pitch angular deflection of the outboard spool relative to the inboard spool. The relationship between θ_c and ϕ is obtained by equating an arc length y as defined by the torsional twist angle and by the pitch angle θ_c :

$$y = l\phi \quad (2)$$

$$y = \sqrt{(r\theta_c)^2 + (\Delta l)^2} \quad (3)$$

where Δl is the change in strap length with angular deflection. The change in strap length is the decrease or foreshortening with θ_c . To evaluate the magnitude of Δl , Δl will be determined by computing the straight line distance between point A and point B in figure 5. It is assumed the strap does not elongate under tension load so distance between point A and point B is the length of the untwisted strap.

$$(X_B - X_A)^2 + (Y_B - Y_A)^2 + (l - \Delta l)^2 = l^2 \quad (4)$$

or

$$\Delta X^2 + \Delta Y^2 + (l - \Delta l)^2 = l^2 \quad (5)$$

Redefining ΔX and ΔY to include θ_c ,

$$\Delta X = r - r \cos \theta_c, \quad \Delta Y = r \sin \theta_c$$

and equation (5) becomes

$$(r - r \cos \theta_c)^2 + (r \sin \theta_c)^2 + (l - \Delta l)^2 = l^2 \quad (6)$$

Expanding equation (6) and rearranging yields

$$(\Delta l)^2 - 2l(\Delta l) + 2r^2 - 2r \cos \theta_c = 0 \quad (7)$$

Solving for Δl using the binomial theorem, the minimum value for Δl is expressed as

$$\Delta l = l - \sqrt{l^2 - 2r(r - \cos \theta_c)} \quad (8)$$

with $\theta = 100^\circ$ and the strap geometry parameters defined as $l = 57.1$ mm, and $r = 6.85$ mm,

$$\Delta l = 0.84 \text{ mm}$$

With Δl defined, equation (3) can be evaluated. For $\theta_c = 100^\circ = 1.745$ rad then,

$$(r\theta_c)^2 = 142.9$$

Since $(r\theta_c)^2$ term is very large compared to $(\Delta l)^2 = 0.706$, the $(\Delta l)^2$ term can be neglected and equation (3) can be simplified to

$$y = r\theta_c$$

Equating arc length y as defined by equations (2) and (9),

$$l\phi = r\theta_c \quad (10)$$

and

$$\phi = (r/l)\theta_c \quad (11)$$

If ϕ is a small angle, then further modifications of equation (1) are simplified. The angle ϕ can be defined from the following expression based on geometry.

$$\begin{aligned} \phi &= 2 \sin^{-1} \frac{\sqrt{2r^2 + (\Delta l)^2}}{2l} \\ &= 9.76^\circ \end{aligned} \quad (12)$$

With ϕ only 9.76° , then

$$\tan \phi \approx \phi \approx (r/l)\theta_c \quad (13)$$

Also, the additional control moment term can be redefined as

$$(dM_{sp}/d\phi)\phi = (dM_{sp}/d\theta_c)\theta_c \quad (14)$$

Substituting equations (11), (13), and (14) into equation (1) yields

$$M_c = [(r^2/l)F_{CF} + (dM_c/d\theta_c)]\theta_c \quad (15)$$

With $\theta_c = \theta_{PT} + \Delta\theta$, then

$$M_c = [(r^2/l)F_{CF} + (dM_c/d\theta_c)](\theta_{PT} + \Delta\theta) \quad (16)$$

Thus, the control moment is expressed in terms of the pitch-angle deflection of the controller outboard end.

In the application of control moment to the free tip, a control moment invariant with tip pitch deflection was the ideal goal. However, the control-moment variation from figure 6, which is 9% of the maximum design value of 6.78 N·m, was acceptable. Also, the $\pm 1.9\%$ variation owing to hysteresis was considered to be acceptable.

The calculated uncoupled blade natural frequencies are presented in figure 7 as a function of rotor speed. These frequencies were calculated using the transfer matrix method. This method employed 25 lumped masses with each mass having 5 degrees of freedom: flapping, lead-lag torsion, flap bending, and chordwise bending. Although these frequencies reflect a fixed-tip configuration, the flatwise and chordwise frequencies are also applicable to the free-tip configuration, since the mass, center-of-gravity location, and moments of inertia properties are the same.

The spanwise distribution of blade mass and its offset from elastic axis are presented in figure 8. Another design criterion was that the tip center of gravity to be on the pitch axis at 0.13 c. Space and volume restrictions presented the achievement of that goal, however, and the tip c.g. was located at 0.14 c. The blade had a 0.171-m chord, a constant V23010-1.58 airfoil, and -9.45° of linear twist from center of rotation out to and including the tip. The free tip had a V23010-1.58 airfoil with a 5.8% chord tab added to match the basic blade airfoil. The 0.1 R tip was constructed of Nomex core and magnesium spar covered with fiberglass. The upper and lower surfaces were covered with 0.013-mm-thick Mylar to prevent air transfer from the lower to the upper surface. For chordwise mass balance, tantalum balance weights were inserted in the space ahead of the pitch axis. Table 1 presents a summary of the rotor dimensional characteristics.

Boeing Vertol's dynamic rotor test stand, which incorporates an electrical power supply and a six-component balance, was used for the test. The test was conducted in the Boeing Vertol 20- by 20-ft V/STOL wind tunnel. The wind-tunnel test section was configured with slotted walls, slotted ceiling, and slotted floor to give 10% porosity for forward flight testing.

Instrumentation for the main blade consisted of four flap-bending gauges at 0.13 R, 0.18 R, 0.38 R, 0.53 R and one chord-bending gauge at 0.18 R. Additional flapwise and chordwise bending gauges were located at 0.9 R and on the base of the shaft about which the tip pitches. Shaft torque was measured using torque gauges on the rotor drive shaft.

Blade-flapping motion about the flap hinge was continuously measured by transducers placed at the flap hinge of the instrumented blade. The angle of the tip

relative to the main blade was measured by a Hall-effect device. In that device, a tiny magnetic on the free tip is used to modulate an electric current through a semiconductor mounted on the inboard portion of the blade.

AERODYNAMIC DESIGN OF THE TIP

The principal aerodynamic design criterion was high C_{m_α} for fast responsiveness to velocity perturbation. For fast responsiveness to velocity perturbation, a minimum value for C_{m_α} of -0.012 was selected. This was based on studies reported in references 2 and 7. In those studies, tip-response characteristics were evaluated for both a simple segment and an integrated system of the rotor plus free tip. Although a $C_{m_\alpha} = -0.012$ was shown to allow sufficient responsiveness to provide performance improvement and reduced vibratory loads, this did not preclude designing to a greater magnitude in C_{m_α} to enable faster response to angle-of-attack perturbation.

The system natural frequency and damping characteristics were expected to be sufficient to negate the possibility of flutter. However, the final planform configuration was expected to have a great influence on the tip damping characteristics, especially when sweep is included.

Aerodynamic design was also influenced by structural requirements. The paramount structural constraints were the flatwise bending moment at the inboard edge of the pitch shaft and the centrifugal force on the controller assembly. These two constraints necessitated tip chord taper to reduce maximum lift capability, to move the spanwise center of pressure inboard, and to lower the weight and the pitch inertia of the tip. Transmittal of the chordwise and flatwise bending moment from the tip to the pitch shaft necessitated the pitch shaft extending to half the span of the tip. This allowed the reaction forces to be within structural limits of the thin-wall tip section, but forced chord taper and sweep to be incorporated only over the outboard 50% of the tip. Tip chord taper of 0.3 was required to satisfy the structural requirements. Sweeping the tip 35° was more than sufficient to meet $C_{m_\alpha} = -0.012$ criterion, as determined from the wind-tunnel test data presented in figure 9.

PRETEST CHECKOUT

Before wind-tunnel entry, the free-tip rotor was run in a test cell to determine experimentally the natural frequency of the free-tip system and to determine if the system was critically damped or underdamped. This would show the quickness of

the free-tip's reaction to flow perturbations. Satisfaction of these quantitative objectives would determine the readiness of the free tip for a wind-tunnel test.

The experimental natural frequency and damping characteristics were determined by analyzing the response to an abrupt change in angle of attack. An abrupt $\Delta\alpha$ input was obtained by driving the blades through a vertical airjet that caused the tip to pitch nose-down. After leaving the air jet, the tip saw an abrupt negative change in angle of attack, to which it responded by pitching nose-up to some equilibrium pitch angle. A schematic of the test setup is presented in figure 10, which also shows the tip angle-of-attack change and the deflection as it passes by the jet. Tip response after leaving the air jet was used to determine frequency and damping characteristics because the air-velocity states were better known. Although the air-velocity characteristics are better known, they cannot be considered analytically constant, because of recirculation in the room. Blade pitch, $\theta_{0.75}$, was varied from 0° to 8° , but this produced considerable recirculation within the test chamber. The recirculation was probably uneven across the rotor disk and around the azimuth. This unevenness was attributed to the rectangular shape of the test cell, the proximity of the rotor to the walls (one wall being about 25% open to the outside atmosphere), and blowing at only one small area of the disk. Experimentally derived frequency and damping characteristics were compared with analytically derived characteristics to evaluate the weathervaning capabilities of the tip.

Analytical Derivation of Tip Dynamic Response

The analytical characteristics were derived using the response of a second-order system. From the free-body model shown in figure 11, the response equation is derived as

$$-I\ddot{\theta}_t - b_A\dot{\alpha}_t - \frac{b_f(\dot{\theta}_t - \dot{\theta}_l)}{|\dot{\theta}_t - \dot{\theta}_l|} - K_\alpha\alpha_t - TR\theta_t + M_c - k(\theta_t - \theta_l) + M_\beta + M_\zeta = 0 \quad (17)$$

where $b_A\dot{\alpha}_t$ is the damping moment produced by aerodynamics that include the effect of tip planform, $[b_f(\dot{\theta}_t - \dot{\theta}_l)]/|\dot{\theta}_t - \dot{\theta}_l|$ is damping from friction forces generated by the tip oscillating about the pitch shaft, K_α is the rate of change of aerodynamic pitching moment with angle of attack, $TR\theta_t$ is the feathering moment produced by centripetal acceleration on the mass located forward and aft of the pitch axis, and where M_β and M_ζ are inertial moments produced by the tip's c.g. offset from the pitch axis in conjunction with flap and lead-lag angles plus their respective velocities and accelerations.

Rearranging equation (7) and including the identity $\Delta\theta = \theta_t - \theta_l$,

$$I\ddot{\theta}_t + b_A\dot{\alpha}_t + \frac{b_f(\dot{\theta}_t - \dot{\theta}_l)}{|\dot{\theta}_t - \dot{\theta}_l|} + K_\alpha\alpha_t + TR\theta_t + k(\theta_t - \theta_l) = M_c + M_\beta + M_\zeta \quad (18)$$

A number of assumptions were made that simplify this moment equation. First, it was assumed that the inboard portion of the blade did not torsionally deflect while penetrating the jet. This is a reasonable assumption since the air jet was focused on the tip itself with little efflux impinging on the inboard portion of the blade, and the inboard section torsional inertia was about 10 times that of the tip. Second, it was assumed the $\theta_{0.75}$ was zero. For this test of tip responsiveness, $\theta_{0.75}$ could have been any value. Zero $\theta_{0.75}$ was selected to minimize recirculation effects. Third, α_t was assumed to be approximately the same as $\Delta\theta$. Fourth, it was assumed that the air jet effects caused no significant blade flapping or lead-lag. Fifth, K_α was assumed to be numerically the rate of change of pitching moment with respect to tip incidence, K_i , rather than with respect to the angle of attack of the blade. This is reasonable since the inboard portion of the blade does not experience the efflux during jet penetration and therefore would not have an angle-of-attack change during that time. Neither would there be an angle-of-attack change on the inboard section coming out of the azimuthal zone of the jet and during the tip response. With the above assumptions,

$$\theta_t = \theta_l = 0$$

$$\alpha_t = \Delta\theta$$

$$\dot{\alpha}_t = \Delta\dot{\theta}$$

$$\beta = \dot{\beta} = \ddot{\beta} = 0, \text{ and therefore } M_\beta = 0$$

$$\zeta = \dot{\zeta} = \ddot{\zeta} = 0, \text{ and therefore } M_\zeta = 0$$

$$K_\alpha = K_i$$

Since $\theta_t = \theta_l + \Delta\theta$ and $\theta_l = 0$, then $\theta_t = \Delta\theta$, $\dot{\theta}_t = \Delta\dot{\theta}$, and $\ddot{\theta}_t = \Delta\ddot{\theta}$. Inserting these terms into equation (8),

$$I\Delta\ddot{\theta} + (b_A + b_f)\Delta\dot{\theta} + (K_i + k + TR)\Delta\theta = M_c \quad (19)$$

This equation was solved using Laplacian techniques which account for initial conditions of $\Delta\dot{\theta} = 0$, $M_c = 0$, and $\Delta\theta_0 = 4^\circ$.

The expression for the response is then determined to be

$$\Delta\theta = \Delta\theta_0 \left[\frac{a}{\omega} e^{-\lambda t} \sin(\omega t + X_1) + \frac{M_c}{I} e^{-\lambda t} \sin(\omega t) \right] \quad (20)$$

where

$$\omega = \left[\left(\frac{b_f + b_A}{2I} \right)^2 - \frac{K_i + k + TR}{I} \right]^{1/2}$$

$$a = \left[(\omega)^2 + \left(\frac{\Delta\dot{\theta}_0}{I\Delta\theta_0} \right)^2 \right]^{1/2}$$

$$\lambda = \frac{b_f + b_A}{2I}$$

$$X_1 = \tan^{-1} \frac{\omega I \Delta\theta_0}{\Delta\dot{\theta}_0}$$

Numerical estimates of the parameters are as follows:

$$K_i = \frac{-dC_m}{d\Delta\theta} c_t S_t \frac{1}{2} \rho (\Omega R)^2 C_1$$

where $dC_m/d\Delta\theta$ is a static value (from R. H. Stroub and J. van Aken, "Tip Aerodynamic Characteristics from a Wind-Tunnel Test of a Semispan Wing," proposed NASA TM) and C_1 is an estimated correction for dynamic oscillation from reference 7. For $dC_m/d\Delta\theta = 0.01$, $\Omega R = 213.4$ m/sec, $C_1 = 0.825$, and the tip geometry $K_i^m = 80.22$ N·m/rad.

The aerodynamic damping coefficient is defined as $b_A = (dC_m/d\dot{\theta})(\rho/4)\Omega R S_t c_t^2$,

where $dC_m/d\dot{\theta}$ is from reference 8. For $dC_m/d\dot{\theta} = 2.6$, $b_A = 0.1734$ N·m/rad/sec. With tip lift load and flapping near zero, then $b_f = 0$, $k = 3.519$ N·m/rad from figure 6, $TR = 0.369$ N·m/rad, and $I = 2.84 \times 10^{-4}$ kg·m² (from geometry).

The coefficients of the response equation (10) are now determined:

$$\omega = 443.18 \text{ rad/sec}$$

$$a = 443.18 \text{ rad/sec}$$

$$\lambda = 314.1 \text{ sec}^{-1}$$

$$X_1 = 1.5708 \text{ rad}$$

After the coefficients are substituted into equation (10) the response equation for 796 rpm, or $\Omega R = 213.4 \text{ m/sec}$, becomes

$$\Delta\theta = \Delta\theta_0 e^{-314.1t} \sin(443.18t + 1.571) = \Delta\theta_0 e^{-314.1t} \cos(443.18t)$$

Likewise, at 740 rpm,

$$\Delta\theta = \Delta\theta_0 e^{-292t} \cos(428.28t)$$

and at 600 rpm,

$$\Delta\theta = \Delta\theta_0 e^{-236.7t} \cos(353.95t)$$

Comparison of Analytical and Experimental Values

From these three analytical response equations, the frequency and damping characteristics will be compared to experimental values determined from the time-histories shown in figure 12 for three rotational speeds. Figure 13 shows the techniques used in determining the frequency and damping characteristics from the experimental data. A comparison of analytical and experimental values is presented below.

rpm	Test		Analytical	
	ω/Ω , per rev	λ	ω/Ω , per rev	λ
796	5.2	159	5.32	314.1
740	5.2	291	5.53	292.0
600	5.45	150	5.63	236.7

Test results showed good agreement with the analytical model for the natural frequency, but damping characteristics did not correlate well. Although damping was less than expected, the free tip was a well-damped system. This test of the free tip's responsiveness showed the free-tip system to be a responsive, stable, and well-damped system ready for a wind-tunnel test. With the free-tip system shown to be underdamped with a damped natural frequency of 5.2, the free-tip rotor was ready for a wind-tunnel test.

TEST CONDITIONS AND PROCEDURES

The prime objective of the wind-tunnel test was to evaluate the free-tip configuration to determine its advantages over a similar fixed-tip configuration. In

order to make an effective comparison, both fixed-tip and free-tip configurations were evaluated at a prescribed propulsive force coefficient and minimized blade flapping, with the rotor lift coefficient or advance ratio being the variable. Rotor lift sweeps were made at $V/\Omega R = 0.3$ and $\bar{X} = 0.05$, with minimized cyclic flapping. These data gave an indication of the maximum lift coefficient attainable with a free-tip rotor. To obtain a comparison with forward speed, an advance-ratio sweep was conducted from 0.2 to 0.4 at $C_L/\sigma = 0.07$, $\bar{X} = 0.05$, and minimized flapping. This provided a simulated speed-power polar at a contemporary design lift coefficient and at a propulsive-force coefficient representing an equivalent flat-plate drag area of a relatively low-drag helicopter. Rotor-tip speed was held constant at 213 m/sec, the normal tip speed for this rotor. In addition to the standard advance-ratio sweep, the free-tip-rotor test envelope was expanded to include advance ratios down to 0.1 in order to test the tip's behavior in that turbulent environment.

Data from this test were limited because of resonance problems in the test rig itself. The rig developed an in-plane resonance part way through the test. With the blades off, the resonance was found to be sensitive to rpm, with the test rpm of 796 being very near the amplification peak. In addition, amplification increased further when the rotor shaft was tilted forward from the zero shaft-angle position. The resonance amplification was reduced to zero at 552 rpm, which is a tip speed of only 147 m/sec. This tip speed was too low to permit the obtainment of valid rotor performance and loads information suitable for realistic evaluation of this free-tip configuration. For evaluation purposes, lower tip speed does not enable evaluation of compressibility effects, which are significant contributors to the tip's aerodynamic moment characteristics. Because data for 147-m/sec tip speed does not include compressibility effects, the only useful test data are limited to the 213-m/sec data set included herein.

The procedure for setting each data point was as follows: (1) set rotor tip speed and desired advance ratio, and (2) adjust collective pitch, cyclic controls, and shaft angle to achieve desired rotor lift and propulsive force coefficient, and to minimize first-harmonic flapping. All these dependent variables were visually displayed in real time for the rotor pilot to use in setting the test point.

DATA CORRECTIONS AND PRESENTATIONS

The data output from this test reflect corrections for hub tares. Hub tares were obtained from blades-off testing over the range of dynamic pressures and shaft tilt angles used in blades-on testing. Included in the hub tares were the interference effects of the nonmetric test rig on the hub drag itself. Hub tares did not include effects of the rotor downwash.

No wind-tunnel wall corrections were applied to the data, but blockage corrections were applied to correct free-stream velocity. The rotor power data presented herein reflects standardized trim conditions based on propulsive force level and

lift level when appropriate. Corrections were applied to the data to compensate for small increments from the standardized conditions. The applied corrections are presented as follows:

1. To correct for rotor lift increment from $C_L/\sigma = 0.07$:

$$\frac{\Delta C_p}{\sigma} = \left[(0.07)^2 - \left(\frac{C_L}{\sigma} \right)^2 \right] \frac{\sigma}{2V/\Omega R}$$

2. To correct for rotor propulsive force increment from $\bar{X} = 0.05$:

$$\frac{\Delta C_p}{\sigma} = (0.05 - \bar{X}) \frac{2(V/\Omega R)^3}{\pi}$$

Since test lift and propulsive force values were very close to the standardized condition, corrections were 1% or less for the whole test.

Dynamic loads, bending moments, and tip-deflection angles are the averaged data taken over ten rotor revolutions. The averaged data were then processed to determine mean values, peak-to-peak amplitudes, and harmonic content. Figures depicting tip $\Delta\theta$ variation around the azimuth are the data for one revolution repeated over two revolutions. This was done to aid visualization over the azimuthal sector between 270° and 90°.

RESULTS

Tip Pitching Behavior at $V/\Omega R = 0.305$

The free tip's weathervaning capability produced pitch angle time-histories that demonstrate the varied aerodynamic environment in which it operates. Figure 14 shows the azimuthal variation of the tip's $\Delta\theta$ over two rotor revolutions at an advance ratio of 0.305 and for various rotor thrust coefficients; rotor propulsive force coefficient was held constant at 0.05. The $\Delta\theta$ has a general overall negative magnitude which was probably caused by a combination of controller output moment (6.0 N·m) and local flow conditions. The tip was probably still producing positive lift, but less than it would had it been fixed.

The free-tip weathervaning enabled it to provide easy identification of vortices it may have encountered. To accomplish this, it must be assumed the tip encounters a shed vortex with counterclockwise rotation. The encounter is such that the counterclockwise rotation results in the tip experiencing a downward velocity increment first and an upward velocity increment second. This order of velocities encountered causes the free tip to pitch up at it approaches the vortex center and then pitch down as it retreats from the center. Therefore, an encounter with a counterclockwise vortex would be identified by a positive $\Delta\theta$ increment followed by

a negative $\Delta\theta$ increment. Figure 14 may show an example of this response at about $\psi = 75^\circ$ when $C_L/\sigma \leq 0.07$. Over a 45° azimuthal region centered at $\psi = 75^\circ$, the $\Delta\theta$ trace has small undulations. With increasing C_L/σ , the undulations, or waviness, become more severe. For two reasons, this growth in waviness with C_L/σ could be indicative of a vortex encounter:

1. The strength of the encountered vortex is directly related to the rotor thrust level: the higher the rotor thrust, the stronger the vorticity.
2. The rotor-tip-path plane was tilted more aft at high C_L/σ than at low C_L/σ in order to maintain the same propulsive force at both thrust levels. With more aft tilt, a rotor blade is closer to a previously generated vortex, and greater vortex induced velocities are encountered.

These two effects often combine where, at higher C_L/σ , the vortices generated are stronger, have higher velocities, and are closer to the tip-path plane. Now, if the free tip were to encounter these vortices, the tip $\Delta\theta$ trace would exhibit a growth in waviness with increasing C_L/σ . Therefore, the increased waviness exhibited at about $\psi = 75^\circ$ suggests that a tip vortex was encountered.

Harmonic analysis of the free tip's waveform is presented in figure 15. The 1 per rev dominates by far, with the higher harmonic terms being of the order of 0.5° or less. The magnitude of the 1 per rev is seen to be proportional to the rotor lift coefficient.

We have seen the tip's $\Delta\theta$ azimuthal and harmonic characteristics for a C_L/σ sweep at $V/\Omega R = 0.3$. With some variation owing to possible blade-vortex encounters, the general character of these time-histories was nearly the same for all lift levels. This relative equivalence for all C_L/σ is a result of the general flow state being virtually established by the advance ratio, making variation with C_L/σ a secondary influence. With variation in advance ratio, the situation is different.

Tip Pitching Behavior with Advance Ratio

The tip's $\Delta\theta$ azimuthal characteristics with advance ratio are depicted in figure 16. The waveform for $V/\Omega R = 0.1$ shows what happens when the tip encounters two large disturbances, one at about $\psi = 72^\circ$ and the other at about $\psi = 320^\circ$. One or both of these disturbances may be a tip vortex shed from a previously passing blade. This is particularly possible at the region around $\psi = 72^\circ$. The response of the tip to these disturbances is quick and stable. With increasing advance ratio, the tip's response diminished in these two azimuthal regions. This suggests that the intensity of both disturbances was also reduced, and the disturbances nearly disappeared at $V/\Omega R = 0.3$. Only a small remnant of the effects of the third-quadrant disturbance remains. The peak-to-peak amplitude of the overall trace also diminishes, with advance ratio increasing to 0.3. Beyond $V/\Omega R = 0.3$, the peak-to-peak amplitude increases again. These amplitude increases are due to the large changes in the basic aerodynamic environment associated with higher-speed

flight. The tip's $\Delta\theta$ becomes more positive on the advancing side near $\psi = 120^\circ$ as the inboard portion of the blade reduces pitch to achieve rotor trim. On the retreating side at about $\psi = 270^\circ$, the $\Delta\theta$ becomes more negative, as cyclic pitch drives the inboard section to higher pitch angles for rotor trim.

In figure 16, the waveform for $V/\Omega R = 0.1$ also demonstrates the high-pitch-rate generating capability of the free tip. The pitch rate of $1857^\circ/\text{sec}$ (32.4 rad/sec) is inferred by the 10.5° $\Delta\theta$ change that occurred over a 27° azimuthal increment centered at about $\psi = 72^\circ$.

Figure 17 presents a compilation of the $\Delta\theta$ waveforms for all the advance ratios. This compilation shows the aerodynamic environment changing over different sectors of the rotor disk, as the rotor is at various forward speeds.

The harmonic content of the tip's differential pitch angle varied considerably with advance ratio. Figure 18 shows this variation. At $V/\Omega R < 0.2$, the tip response has significant content in harmonics 1 through 8, with the first and second harmonics having the largest absolute magnitude. The remaining harmonics, 3 through 10, taken as a complete group, reflect considerable growth with decreasing advance ratio. This growth is probably a result of the free tip coming closer to, or encountering, tip vortices shed from the previous passage of a blade. This is suggested by the waveforms shown in figure 19, where only harmonics 3 through 10 were summed to produce waveforms for $V/\Omega R = 0.1$ to 0.2 . At these low advance ratios, the suspected influence of shed vortices is very strong, because the tip-path-plane tilt is very low and the strength of the tip vortex is very high. Therefore, the higher harmonic content of the $\Delta\theta$ waveform is probably a result of the proximity of tip vortices when the advance ratio is less than 0.2 .

With advance ratios greater than 0.2 , there is continued growth and dominance of the first harmonic content (fig. 18). It is likely that at least part of this growth was caused by the increase in longitudinal cyclic pitch being impressed upon the inboard portion of the blade. While the inboard pitch is being increased by cyclic pitch, the free tip appears to nullify that increase in longitudinal cyclic.

Figure 16 shows that at $V/\Omega R = 0.391$, $\Delta\theta$ has a large negative value at $\psi = 270^\circ$ when longitudinal cyclic pitch is driving the inboard blade to a maximum value. Keep in mind that the tip is programmed to attempt to maintain nearly uniform lift around the azimuth and, therefore, it needs a high angle of attack at $\psi = 270^\circ$, as does the rest of the blade. Also note that the rotor disk is tilted forward 5° . When the rotor tilt is added to the local downwash angle, there is a negative inflow angle, perhaps of the order of -8° to -10° . And when that negative inflow angle is added to the 9° absolute pitch angle at $0.95 R$ (from rotor control settings), the net is about 0° pitch angle or a 0° effective angle of attack for the free tip. But if the effective angle of attack is 0° , how could the tip be lifting? Probably the tip is lifting because a positive control moment was being applied to the controller. If the tip is lifting, two events are occurring, either singularly or in combination: either the inboard portion of the blade is experiencing dynamic twist that is of the order of 7° nose-up at $V/\Omega R = 270^\circ$, or the high C_L of the inboard blade caused a large upflow at the tip. Unfortunately, neither

event can be ascertained from the test data. Both events are probably occurring, however, to a lesser degree. It would be well to establish the dynamic twist of the blade in the next wind-tunnel test.

In figure 18, the second harmonic magnitude decreased with increasing advance ratio until $V/\Omega R = 0.3$, and then it increased again. The magnitudes of harmonics 3 through 10, taken as a group, had the usual expected distribution as advance ratio increased to 0.3. At advance ratios beyond 0.3, the magnitude of harmonics 4-6 grew larger. No particular significance can be attached to the changes in higher harmonic magnitudes at this time.

Oscillatory Lift Calculation

The motion of the free tip is in response to changes in the aerodynamic environment that produce oscillatory lift loading in a fixed-tip configuration. A question arises as to how much loading change is alleviated by the free tip. This question is answered by reviewing an analytical loading calculation based on the tip pitch angle and on the local velocity normal to the tip. The primary hypothesis here is that all $\Delta\theta$ tip response is generated by lift-loading perturbations. The analytical expression used to define the lift loading is

$$\text{Loading} = C_{L_\alpha} \Delta\alpha S_t 0.5\rho V^2 \quad (21)$$

$$\text{Loading} = C_{L_\alpha} \left[A_0 + \sum_{N=1}^{10} (A_N \sin N\psi + B_N \cos N\psi) \right] [\Omega R(1 + \mu \sin \psi)]^2 0.5\rho S_t \quad (22)$$

$$\text{Loading} = 0.5\rho S_t C_{L_\alpha} [(\Omega R)^2 + 2\mu(\Omega R)^2 \sin \psi + (\mu\Omega R)^2 \sin^2 \psi] \left[A_0 + \sum_{N=1}^{10} (A_N \sin N\psi + B_N \cos N\psi) \right] \quad (23)$$

where

$$\Delta\theta = A_0 + \sum_{N=1}^{10} (A_N \sin N\psi + B_N \cos N\psi)$$

is assumed equal to $\Delta\alpha$.

The lift curve slope, C_{L_α} , reflects the situation that the whole tip, and at least part of the inboard section of the blade, are subjected to the local angle-of-attack change. Also, the C_{L_α} reflects a lift deficiency factor of 0.827 for

consideration of unsteady aerodynamics. Using $C_{L\alpha} = 0.065$ per degree from Stroub and van Aken and $C_l = 0.827$ from reference 8, the effective $C_{L\alpha}$ is 0.0537 per degree. Based on this effective $C_{L\alpha}$, the resulting calculated lift loading per unit tip area, that is, the lift loading parameters, is presented in figure 20 for two rotor lift coefficients, $C_L/\sigma = 0.0708$ and 0.0915 at $\bar{X} = 0.05$ and at an advance ratio of 0.305. The loadings for the two lift levels are about the same in character but different in magnitude. The negative values shown reflect a response to a positive change in local angle of attack. Likewise, positive values represent a response to a negative angle-of-attack change. These data show the tip reducing the loading around the azimuth, with the larger reduction on the retreating side of the rotor disk. More important though are the changes related to higher harmonic loading, which contributes to vibratory loads in the nonrotating system. The fixed-system vibratory loads are affected by higher harmonics above 2 per rev and, mainly, by harmonics 3 through 10 per rev. Calculated higher harmonic air-load changes caused by the free tip are depicted in figure 21 as the summation of magnitudes and phases of harmonics 3 through 10 at two rotor lift coefficients. At $C_L/\sigma = 0.0708$, the resulting curves show the largest perturbation occurring over an 80° azimuthal sector centered at about 0° azimuth. The major discernible effect with rotor lift coefficient is that higher lift appears to increase the amplitude of lesser peaks. The maximum overall peak-to-peak amplitude was not changed, but there are more high magnitude peaks occurring at $C_L/\sigma = 0.0915$ than at $C_L/\sigma = 0.0708$.

The same approach was taken for the free tip at different advance ratios. Figure 22 presents the calculated total air loading for $C_L/\sigma = 0.0708$, $\bar{X} = 0.05$, at advance ratios of 0.305 and 0.392. In figure 23, harmonics 3 through 10 are summed and presented for the same two advance ratios. Increasing the advance ratio from 0.305 to 0.392 changes some peaks around the azimuth, but the biggest effect is the amplitude change over the front part of the disk, at about the 180° azimuth. The greatest potential for aerodynamically induced oscillatory loads appears to come from the fore and aft sector of the disk and from the advancing-blade zone centered near 120° azimuth. With this approach, we are able to identify areas that might be major sources of the vibratory loads that affect fixed-system vibration.

Even at near-equivalence in force and speed settings, the free-tip lift loading parameter shows considerable variation between the data from the lift sweep in figure 21 and the data from the speed sweep in figure 23. Figure 24 presents the lift-loading parameter from figures 21 and 23 for $C_L/\sigma = 0.0708$, $\bar{X} = 0.05$, and $V/\Omega R = 0.3$. At near-equivalence in force and speed setting, the character of the harmonic content shows large, distinct differences, especially at 100° azimuth. The data from the lift sweep show that the advancing blade produces a 40% greater peak-to-peak amplitude than the other case. This suggests that small differences in orientation of the tip-path plane can greatly change the aerodynamic environment through which the tip must pass. This would make the synthesis of that aerodynamic environment a difficult task and its validation more difficult as well.

CORRELATION WITH THEORY

A rotor mathematical model was modified to include the free tip. This mathematical model incorporated blade-element theory, an unsteady aerodynamics model, a modal approach to structural dynamics, and a prescribed wake with nonuniform downwash. The model was run to match a wind-tunnel test condition of an advance ratio of 0.3 with the rotor at $C_L/\sigma = 0.07$, $\bar{X} = 0.05$, and a tip speed of 213 m/sec. The correlation between the test data and the model is shown in figure 25, with tip $\Delta\theta$ azimuthal variation being the correlation parameter; the correlation is very poor. The differences between test and model are so large that this mathematical model could not be used in the evaluation of the results of this test.

We have seen the responsiveness of the free tip to airflow perturbation and have examined how it changes its loading characteristics around the azimuth. Next, let us see what are the benefits of its free pitching capability--how it affects power required, blade loads, and control loads.

POWER

Comparison at Various Rotor Lift Coefficients

In forward flight, the free-tip rotor required less power than the comparable fixed-tip rotor configuration. This is shown in figure 26 for a C_L/σ sweep at $V/\Omega R = 0.3$. The free-tip configuration required less power for C_L/σ greater than 0.045 and appears to be a more power efficient configuration with increasing thrust. For example, if the free tip were at the same power coefficient associated with the fixed tip at $C_L/\sigma = 0.07$, the free-tip lift capability would be 15% greater. The primary reason the free tip requires less power is the pitch-down or negative $\Delta\theta$ of the tip relative to the inboard portion of the blade.

There are two reasons the negative $\Delta\theta$ reduces the power requirement. First, negative $\Delta\theta$ lowers tip lift owing to just reducing the α_t and, therefore, lowers the induced drag of the tip. Secondly, negative $\Delta\theta$ causes the tip's "drag due to lift" characteristics to be less severe. These two reasons for lower power from lowered tip drag were demonstrated with wind-tunnel test data from a metric tip on a semispan wing (Stroub and van Aken). The tip was mounted on its own six-component strain gauge balance. The drag due to lift characteristics from that test are presented in figure 27 for 30° and for 35° tip sweep angles. The data presented include those at 0° and -5° incidence angles for the 30°-swept tip and at 0° for the 35°-swept tip.

There were no data taken for 35°-swept tip at -5° incidence angle, but trends with incidence angle associated with the 30°-sweep angle are expected to carry over to the 35°-swept-tip configuration as well. The data in figure 27 show the general sensitivity of tip drag with tip lift and show the relief of that sensitivity with a

-5° incidence angle or $\Delta\theta$. The two reasons for reduced drag and power are demonstrated in figure 26 by noting the following: (1) point A is the undeflected tip lift and drag state; (2) point B shows less drag resulting just from reducing tip lift; and (3) point C shows less drag at the same lift when the incidence angle was negative.

From these data it is easily seen that there is a definite drag advantage when the tip is at a negative $\Delta\theta$ but at the same lift. A quantitative perspective is gained from table 2, which shows what happens to tip drag when tip incidence angle is changed from 0° to -5° and when wing lift is equal in both cases. Two wing-lift coefficients are included in table 2. Wing-lift coefficients reflect the lift of the whole wing, including the tip.

Table 2 shows that the tip-drag reduction with wing lift is the same for incidence angles of 0° and -5°. It should be noted that drag of the complete wing was about the same in both cases, or at least within the accuracy of the wing balance. It is likely that the inboard portion of the wing increased its drag level with negative tip incidence angle, but that it approximately balanced out the decreased drag of the tip. Therefore, for a fixed wing, the drag reduction associated with negative tip incidence angle may be of small net consequence. For rotors, the opposite is true. For a rotor, shifting the drag inboard would reduce the radial arm of the drag centroid, causing less power to be required.

The mechanism for reduced tip drag is hypothesized as an interaction between the tip vortex and the deflected tip. With the tip at a strong negative incidence angle, there will be a substantial lift difference between the tip and the inboard portion of the wing. This lift difference would not be accommodated in a gradual spanwise lift gradient, but there would be a sharp lift discontinuity with the largest gradient at the junction between the tip and the inboard wing. This large gradient in spanwise lift distribution causes a vortex to be shed from that juncture. The shed vortex induces an upwash which causes the tip lift vector to be inclined more forward, thus reducing the induced drag.

Another factor is that the tip incidence angle itself also contributes to tip drag reduction. With a negative incidence angle at the tip, the upper surface of the airfoil is inclined more forward. The suction surface pressures, associated with tip-vortex sweeping the airfoil's upper surface, which is not included more forward. Thus, a lower tip drag would result. Both the effect of the upper-surface inclination and the effect of vortex shed from the juncture would be predominately proportional to the lift coefficient of the wing, not the lift coefficient of the tip itself.

A negative incidence angle at the tip, or $-\Delta\theta$, lowers the tip drag on the semispan wing, and likewise lowers the drag of the tip on the rotor and reduces the rotor's power needs as well.

Comparison at Various Forward Speeds

Speed power polars for the free- and fixed-tip configuration are presented in figure 28. The polar for the fixed tip has been adjusted to correlate with the fixed tip data in the C_L/σ sweep shown in figure 26. In figure 28 the free tip is shown to require less power than the fixed tip. The reasons for the free tip requiring less power were discussed earlier, and those reasons generally pertain here as well. The one exception is the highest advance-ratio case in which the fixed tip exhibits a sharp increase in power demand. The free tip, on the other hand, exhibits a more gradual increase in power required. The fixed tip's sharp increase in power suggests it is experiencing compressibility effects at the advancing-tip Mach number of 0.83, whereas the free-tip configuration appears less susceptible to compressibility effects, perhaps because it is less loaded. This could be one of the most significant aspects of the comparison between these two rotor configurations: the free tip may be less susceptible to compressibility power rise.

OSCILLATORY LOADS

Comparison at Various Forward Speeds

Loads data from this test are presented to provide insight into the effect of one free-tip configuration on oscillatory blade loads and control-system oscillatory loads. It was found that the free tip reduces most out-of-plane vibratory loads, but not in-plane loads. The reduction of out-of-plane blade loads is shown in figure 29, where half peak-to-peak oscillatory bending moments are presented over the test advance-ratio range. Comparisons are shown for the free- and fixed-tip configurations, using several measurement stations along the blade. For advance ratios greater than 0.25, the free tip is effective in reducing the oscillatory amplitudes 30% or more at stations inboard of 0.53 R. Insight into the vibratory-load suppression is gained by harmonic analysis of the oscillation load. Figure 30 presents the harmonic analysis for the four measurement stations with the rotor operating at an advance ratio of 0.305 and $C_L/\sigma = 0.0708$. Figure 30 shows that the free tip markedly reduced the first- and second-harmonic bending moments. Other harmonics were reduced as well, but the third, sixth, and eighth harmonics were increased somewhat. Although some harmonics were increased, the large suppression of the first harmonic played a dominant role in reduced peak-to-peak amplitude

In figure 29, a rise in peak-to-peak amplitude is shown for both tip configurations at advance ratios greater than 0.35. This was probably a reaction to compressibility effects that had similarly increased the power required. At advance ratios less than 0.25, the inboard measurement stations report a rise in free-tip oscillatory load, especially around $V/\Omega R = 0.1$. This rise is probably a result of an encounter with strong tip vortices, as indicated by the $\Delta\theta$ response at about $\psi = 80^\circ$ and 320° in figure 16. Unfortunately, data were not obtained on the fixed-tip blade at the low advance ratios. However, helicopter flight-test data have shown that the fixed-tip blade undergoes a large rise in oscillatory loads at the

lower advance ratios, and one can only guess whether the fixed-tip oscillatory loads would be greater or less than those of the free-tip configuration. Nevertheless, the free-tip weathervaning capability needs to be enhanced through new design.

Comparison at Various Lift Coefficients

We have seen that the free-tip suppresses oscillatory flatwise bending moments at cruise speed and at high speed. We will now review the free-tip's suppression of oscillatory loads at lift coefficients with the advance ratio held constant at 0.305. Figure 31 presents half peak-to-peak flatwise bending moment from various measurement stations for both tip configurations. Rotor propulsive force and advance ratio were held constant while thrust level was varied. The data of figure 31 show that the free tip caused oscillatory load reduction only at measurement stations inboard of $r_p/R = 0.53$. Also, more reduction resulted at the lower rotor lift levels. One reason the free tip could be more effective at the low lift levels was that the rotor disk is tilted more forward at the low lift. By tilting forward, the rotor tip operated farther from the main part of the rotor wake, thus reducing the high harmonic content of the perturbations in the velocity vector. With the resulting increased dominance of the lower harmonics, this particular free tip can pitch effectively to deal with the oscillatory loads. At higher thrust levels, the rotor disk is tilted more aft and operates closer to its wake and its influences. This subjects the tip to higher harmonic velocity perturbations, only some of which the free tip could effectively counter.

Blade chordwise bending-moment measurements were limited to one inboard station at 0.18 R. The measurements for both the free- and fixed-tip configurations are presented in figure 32 for the forward speed sweep and in figure 33 for the rotor lift sweep. The speed sweep data set shows the free-tip configuration producing generally larger oscillatory loads than the fixed-tip configuration, except at $V/\Omega R = 0.3$. At $V/\Omega R = 0.3$, the fixed- and free-tip oscillatory loads for $C_L/\sigma = 0.07$, $\bar{X} = 0.05$ are nearly the same. The rotor lift sweep data in figure 33 confirm this near-equivalence at $C_L/\sigma = 0.0708$ but it also shows the free tip having higher oscillatory loads when $C_L/\sigma > 0.0708$. Evaluating these limited data from this test suggests that the free tip generally increases oscillatory chordwise bending moments over the most important segments of the test envelope. Reasons for the free tip generating the higher chordwise bending moments are not discernible from the available data.

Tip Oscillatory Loads

Sufficient oscillatory loads data were not obtained that would allow comparison between free-tip and fixed-tip configurations. Oscillatory loads were obtained from strain gauges applied to the pitch shaft and just inboard of the inboard edge of the tips. Although the instrumentation was the same for both tip configurations, this instrumentation was sufficient to measure the free-tip oscillatory load but not for

the fixed-tip loads measurement. The missing information is loads data from the pin used to prevent the tip from pitching.

For the free-tip configuration only, the half peak-to-peak flatwise bending-moment amplitudes are presented in figure 34 for the lift sweep and for the speed sweep. In the speed sweep, the sharp decrease in magnitude for $V/\Omega R$ greater than 0.1 may be the result of departing the speed domain of severe blade-vortex interaction. In general, the flatwise bending moments are more sensitive to speed variation than to lift variation.

Control System Oscillatory Loads Comparison

The free tip reduces the oscillatory loads going into the control system via the pitch link. This is shown in figure 35 where peak-to-peak oscillatory pitch-link loads are presented for the advance-ratio sweep and for a lift coefficient sweep at 0.305 advance ratio. As shown in figure 35, as either lift or speed increases, the free tip causes large reductions in oscillatory loads. The high oscillatory loads associated with the fixed tip may be the result of the tip's aft sweep. With aft sweep, the fixed tip's aerodynamic center is aft of the elastic axis, and, therefore, any air-load perturbation in the vertical direction feeds directly into the pitch link, resulting in an oscillatory load going into the control system. The swept tapered tip would therefore make the control system more sensitive to flow states that contain considerable velocity perturbations, such as those encountered when operating at high speed or at high thrust levels. High oscillatory loads from aft sweep are substantiated by a wind-tunnel test of full-scale rotors with various tip shapes, a rectangular and a swept tapered tip being two of the tip planforms tested (ref. 9). Those test results show the control-system oscillatory loads to be more sensitive to lift level with the swept tapered tip than with the rectangular tip, in the absence of significant compressibility effects. Therefore, higher oscillatory loads into the control system can be expected with a fixed-swept-tip configuration. Conversely, a free pitching-moment balancing, swept tip suppresses oscillatory loads going into control system.

Overall Oscillatory Loads Picture

The loads data presented herein are limited, but still they provide insight into the effects of this free-tip configuration. With the free tip, inboard blade stations experienced lower oscillatory flatwise bending moments when the advance ratio was greater than 0.2. Harmonic analysis of the bending-moment data showed that the improvement came largely from suppression of the first harmonic loading. Below an advance ratio of 0.2, the oscillatory loads rose for the free-tip configuration, but no comparison was possible since the fixed-tip configuration was not tested at the lower advance ratios. The oscillatory load rise was attributed to blade-vortex interactions characteristic of that advance-ratio regime. The free-tip configuration generally caused chordwise loads to increase at rotor lift levels above $C_L/\sigma = 0.0708$ and at most speeds tested. Concerning loads going into the

control system, the free tip caused large decreases in pitch-link loads at all lift levels and advance ratios.

CONCLUSIONS

An extensive research program was carried out to analyze and evaluate a free-tip rotor system. The aerodynamic configuration of the free tip was investigated, and there was a successful wind-tunnel demonstration of the free-tip design.

Based on the results of this test and on subsequent data analysis, the following conclusions are drawn. First, the free-tip assembly pitched freely in response to air-flow perturbation. Second, the controller mechanism operated successfully throughout the test program without failure. Third, the free tip reduced power requirements with increasing rotor lift coefficient; at the same power coefficient associated with the fixed tip at $C_L/\sigma = 0.0708$, the free-tip C_L/σ was 15% greater. Fourth, compared with the fixed-tip configuration, the free tip reduced power requirements by about 8% at an advance ratio of 0.3; high-speed power requirements were reduced more. Fifth, with the free tip, blade flatwise bending moments were reduced over the inboard portion of the blade; chordwise bending moments were not reduced. And sixth, the free tip resulted in fewer oscillatory loads being transmitted into the control system.

The free tip will be further developed to exploit its unique capabilities for improving performance and reducing alternating loads.

REFERENCES

1. Stroub, Robert H.: A Constant-Lift Rotor for a Heavier-Than-Air Craft. U.S. Patent 4,137,010, Jan. 30, 1979.
2. Stroub, Robert H.: Performance Improvements with the Free-Tip Rotor. Presented at AHS I-4 National Specialists' Meeting, Rotor System Design, Philadelphia, PA, Oct. 1980.
3. Silcox, H.; and Rosenstein, H.: Feasibility Study of a Constant-Lift Rotor Tip. Report D 210-11704-1, Boeing Vertol Co., Philadelphia, PA, July 30, 1980.
4. McVeigh, M. A. et al.: Investigation of a Rotor System Incorporating a Constant-Lift Tip. NASA CR-166361, 1981.
5. Stroub, Robert H.: An Experimental Investigation of a Free-Tip Rotor Configuration in a Forward Flight Wind-Tunnel Test. NASA TM-84409, 1983.
6. Stroub, Robert H.; and Young, Larry A.: The Results of a Wind-Tunnel Investigation of a Model Rotor with a Free Tip. NASA TM-86758, to be published Aug. 1985.
7. Kumagai, Hiroyuki: A Feasibility Study of Free-Tip Rotor Application as a Passive Cyclic Control Device. NASA CR-166608, 1984.
8. Yates, L.; and Kumagai, H.: Application of Two-Dimensional Unsteady Aerodynamics to a Free-Tip Rotor Response Analysis. NASA CR-166348, May 1982.
9. Stroub, Robert H.; Rabbott, John; and Niebank, Charles F.: Rotor Blade Tip Shape Effects on Performance and Control Loads from Full-Scale Wind-Tunnel Testing. J. American Helicopter Soc., vol. 24, no. 5, Oct. 1979, p. 28.

TABLE 1.- ROTOR GEOMETRIC DESCRIPTION

Rotor radius, m	2.285
Blade chord, m	.1709
Blade twist, deg	-9.45
Tip reference chord, m	.1709
Tip area, m ²	.0322
Tip span, m	.2285
Rotor reference solidity	.0807
Blade flapping inertia, kg·m ²	9.175

TABLE 2.- TIP DRAG REDUCTION WITH
TIP INCIDENCE ANGLE

i_t	C_{L_w}	α_w	C_{L_t}	C_{d_t}
0	0.45	6.0	0.40	0.0300
-5	.45	7.1	.25	.0125
0	.96	12.0	.82	.0670
-5	.96	13.2	.66	.0345

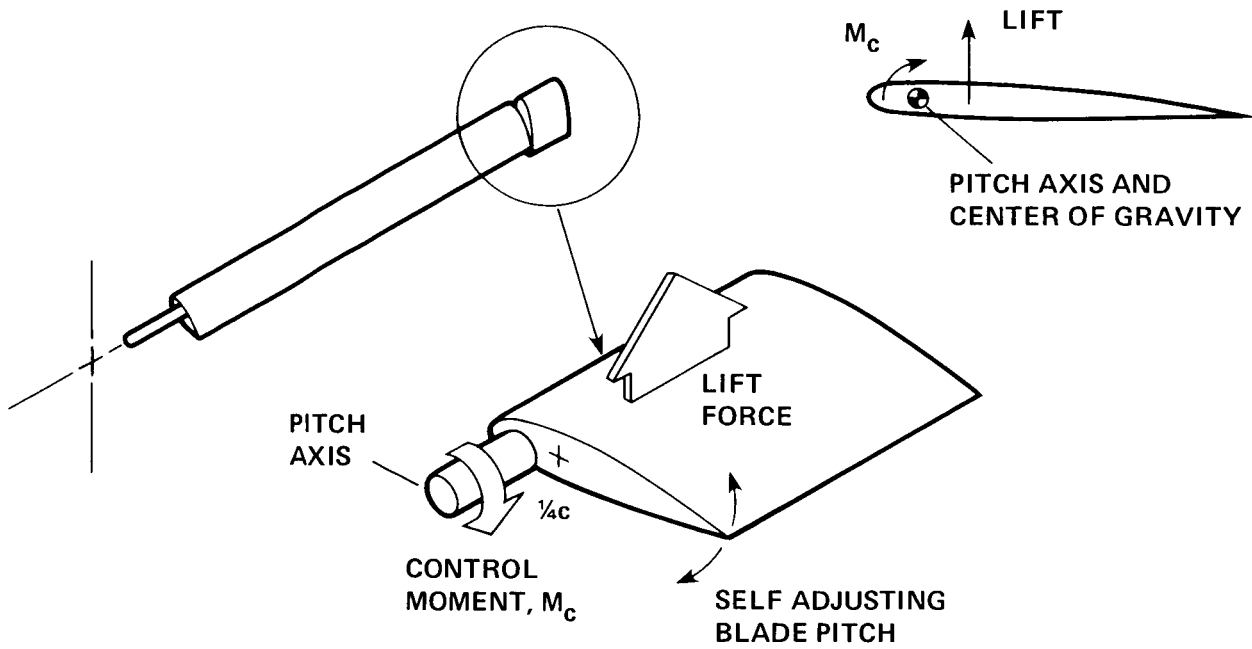


Figure 1.- Schematic of the free tip.

ORIGINAL PAGE IS
OF POOR QUALITY



Figure 2.- Free-tip rotor in Boeing Vertol wind tunnel.

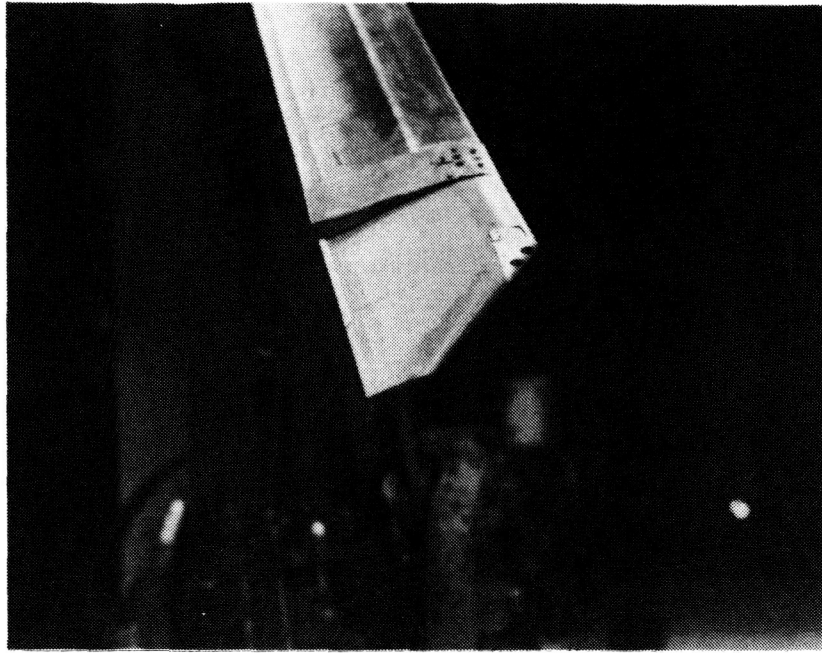


Figure 3.- Close-up view of free tip on rotor blade.

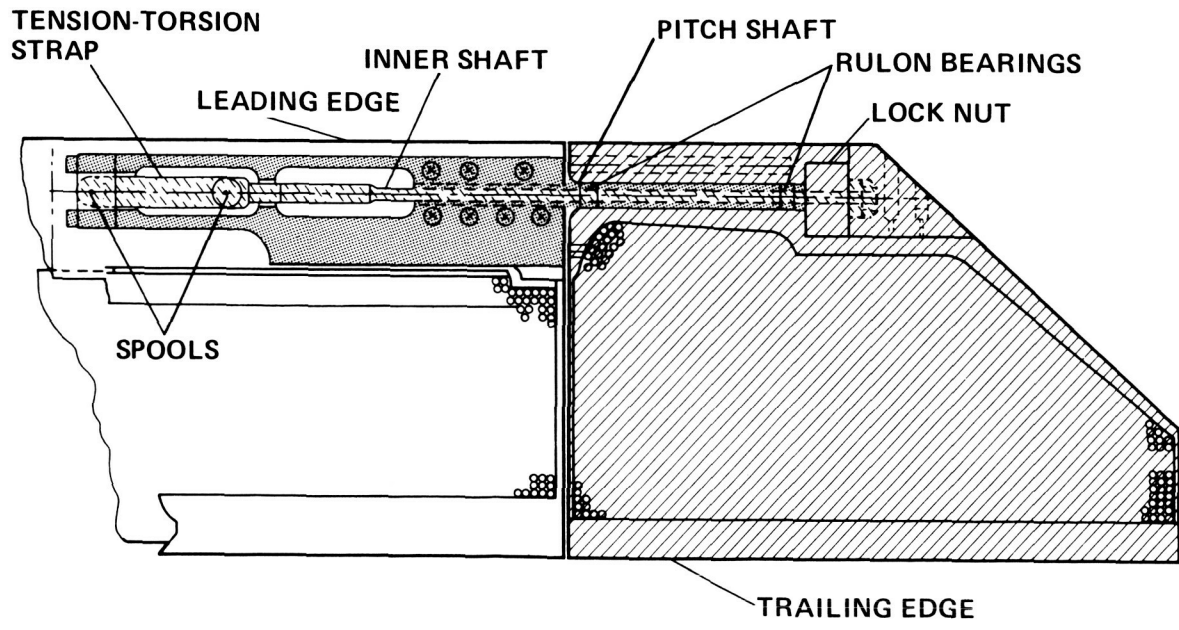


Figure 4.- Free-tip assembly.

ORIGINAL PAGE IS
OF POOR QUALITY

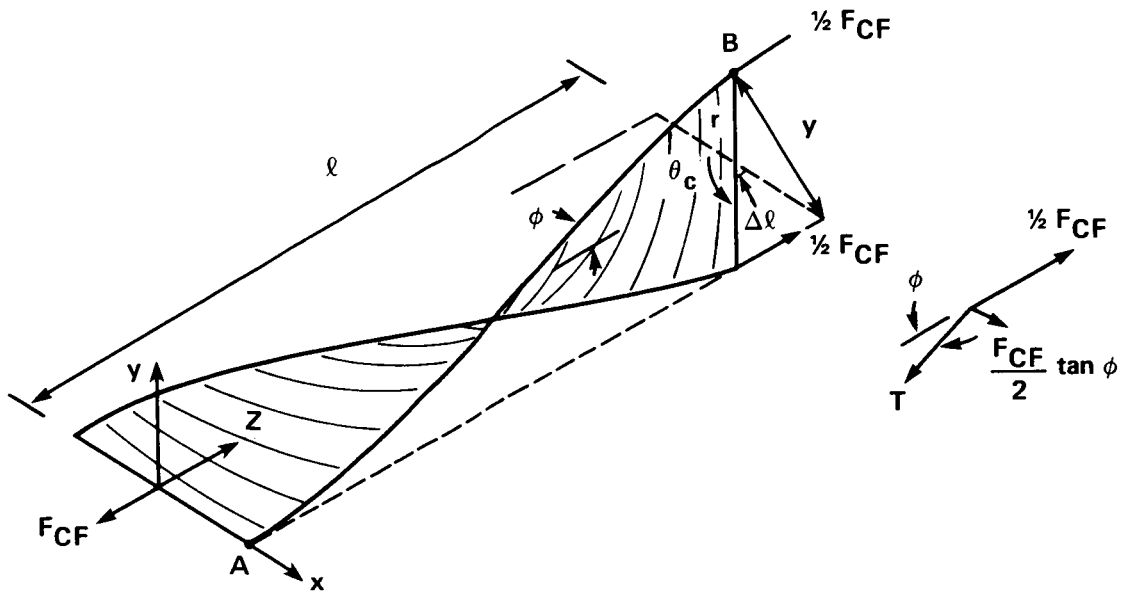


Figure 5.- Free-body diagram of controller tension-torsion strap.

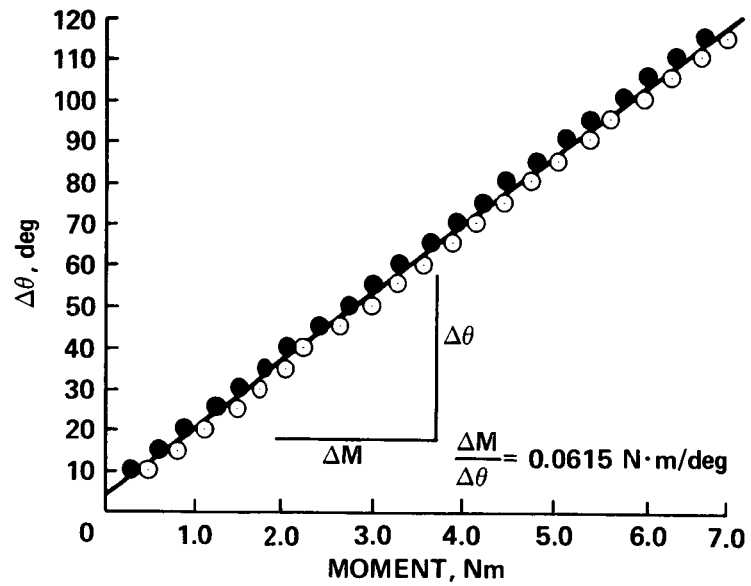


Figure 6.- Torque calibration of controller.

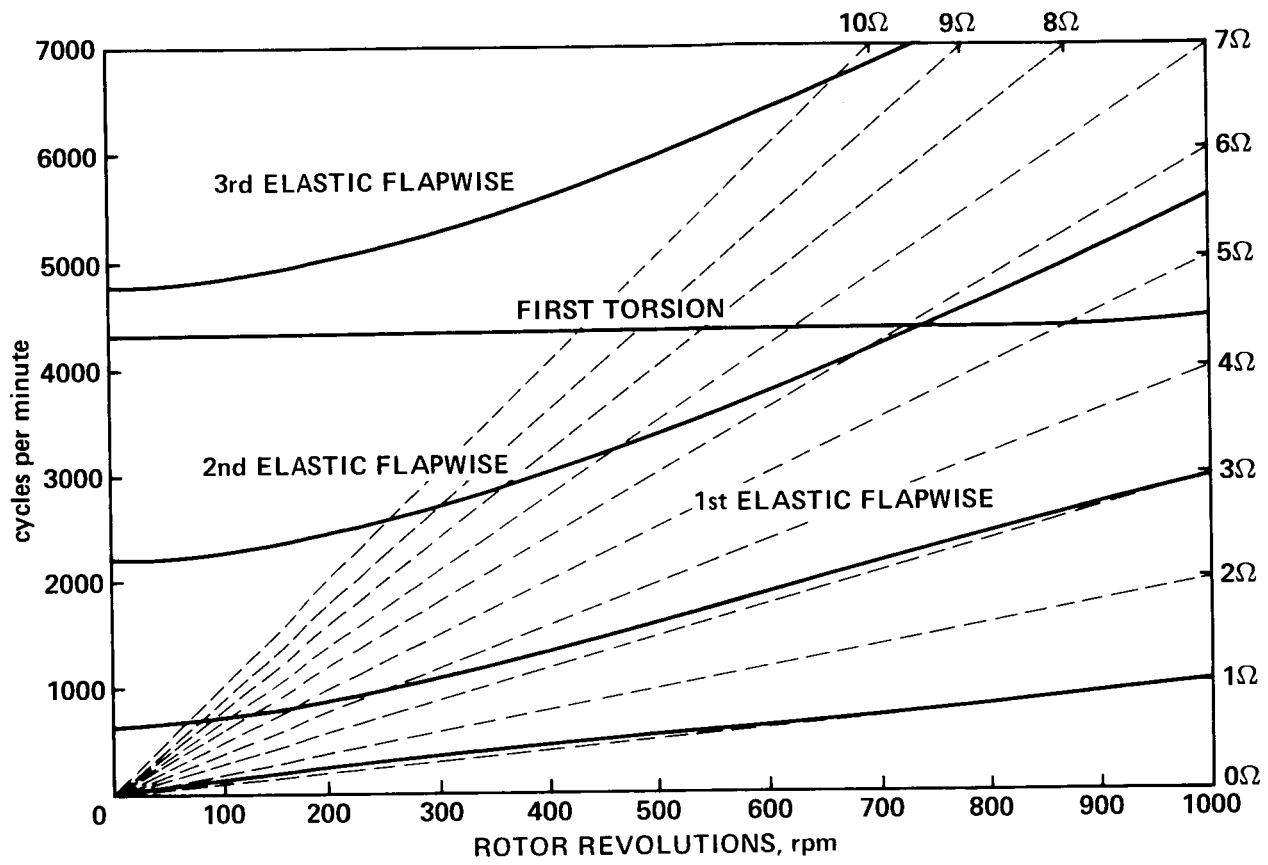


Figure 7.- Rotor-blade natural frequency diagram.

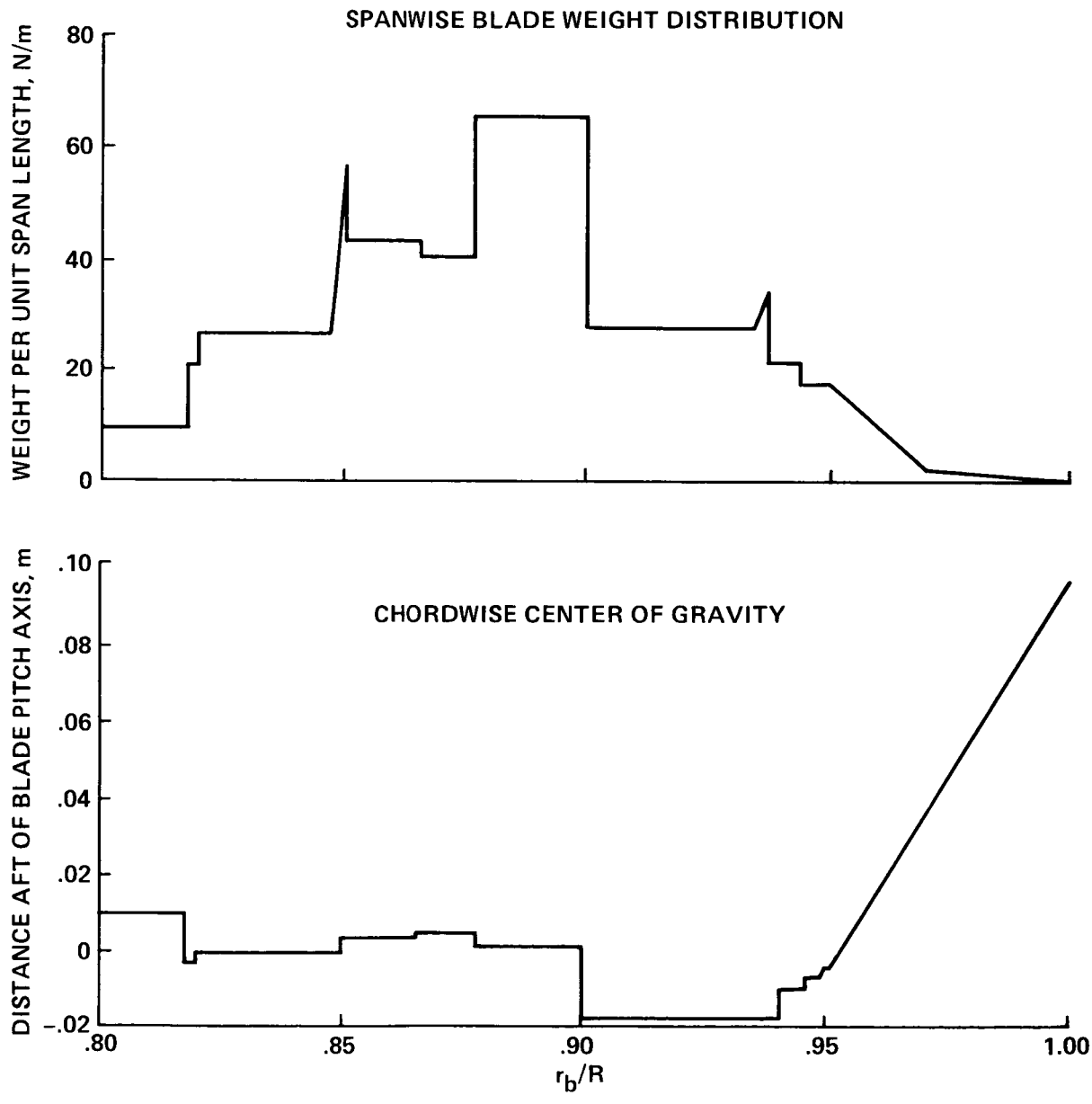


Figure 8.- Mass and center of gravity location of free-tip assembly.

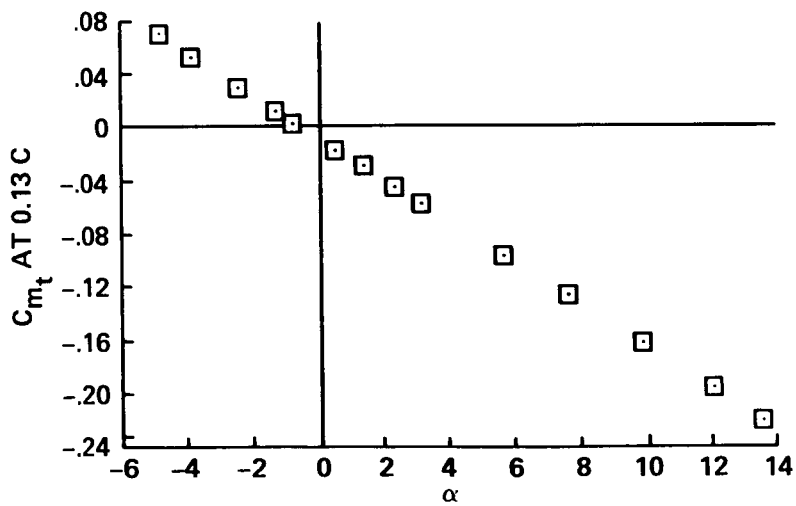
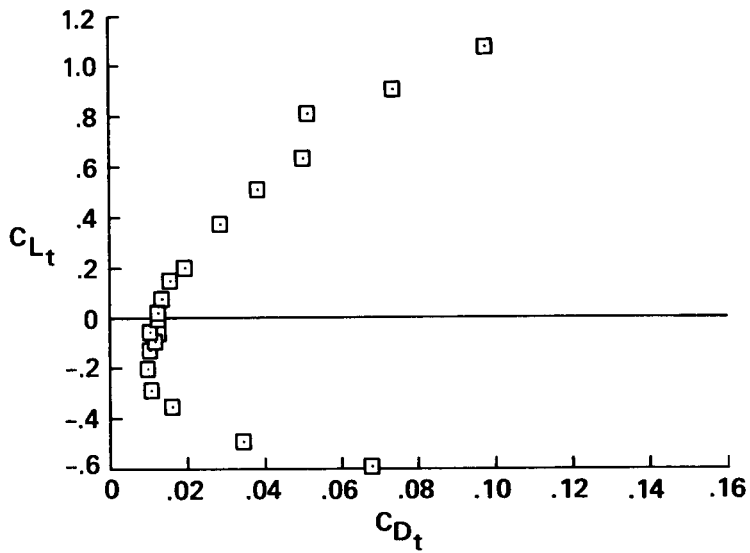
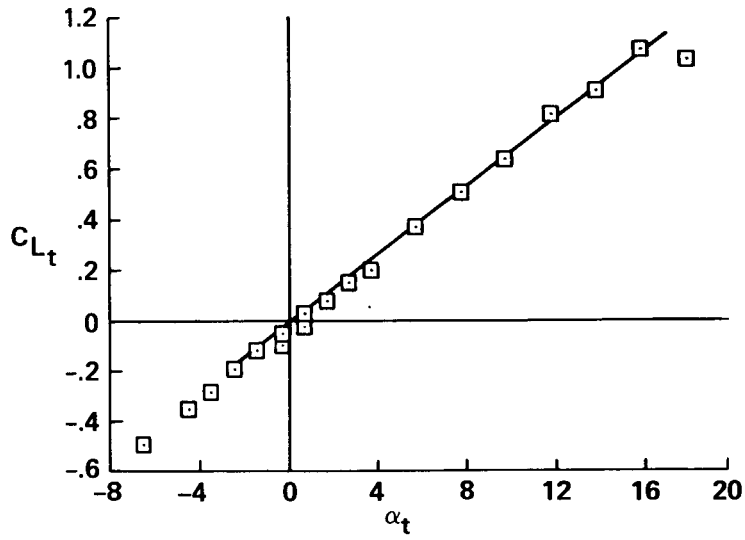


Figure 9.- Aerodynamic characteristics of free-tip planform at Mach 0.17.

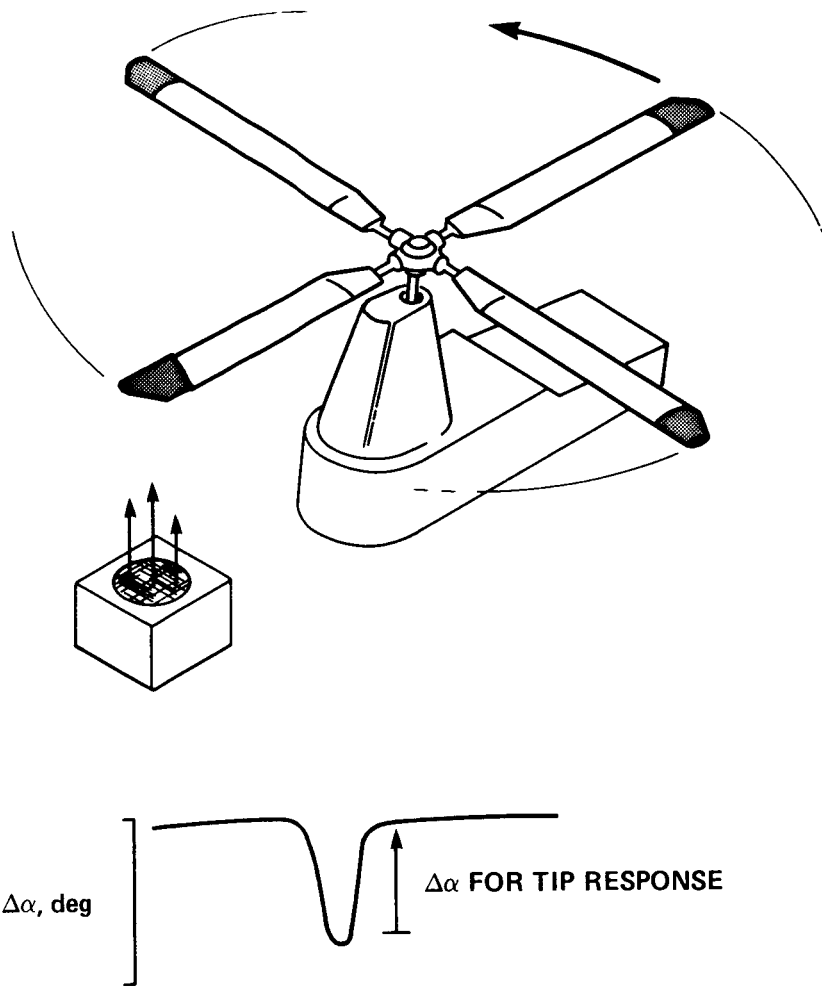


Figure 10.- Free-tip rotor in test cell for test of tip response to a vertical air jet.

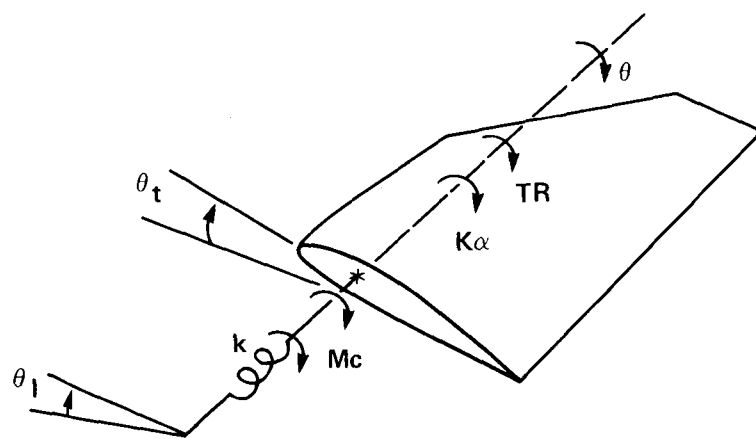


Figure 11.- Free-body diagram of free tip.

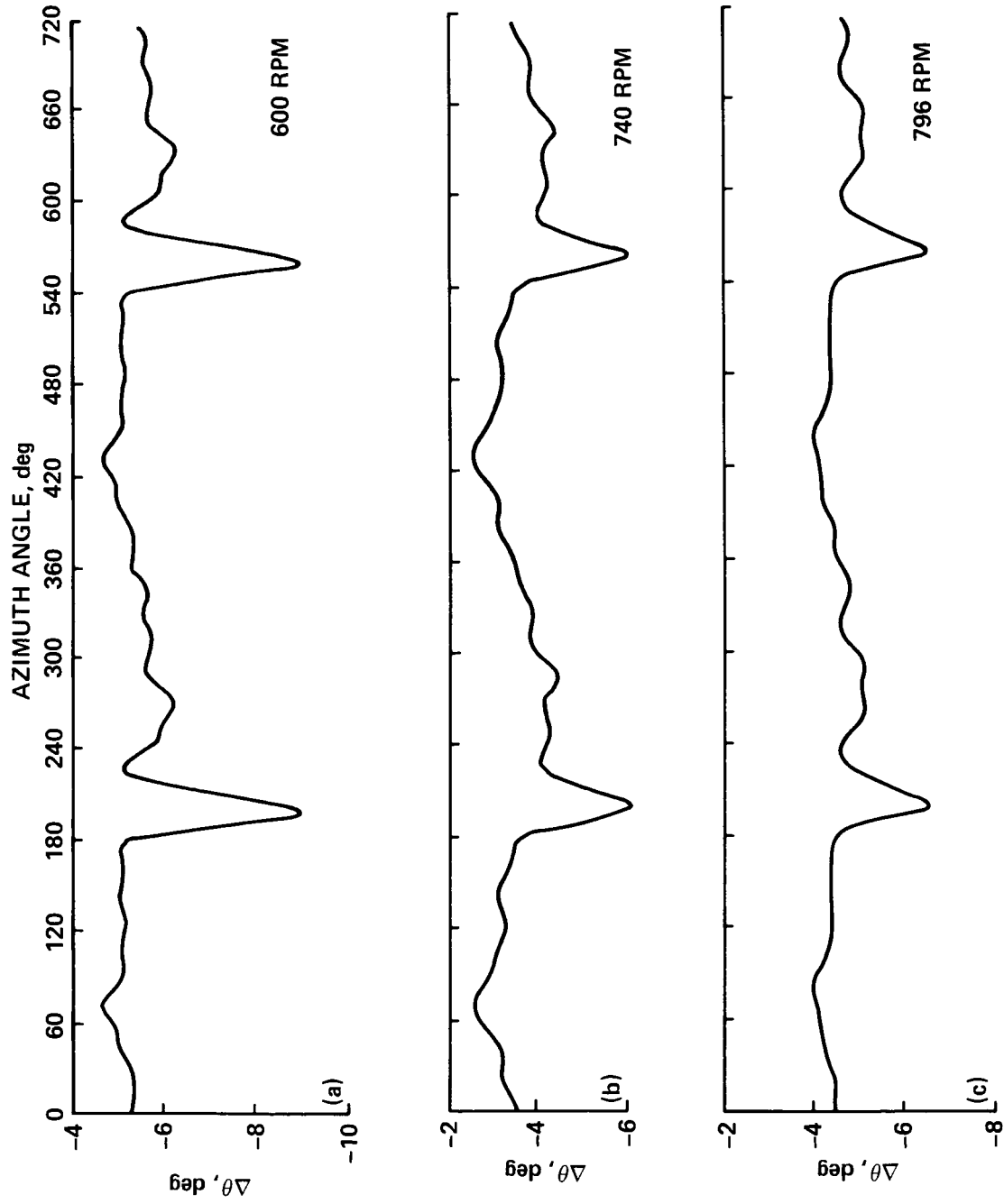


Figure 12.- Time-histories of tip response to a vertical air jet.

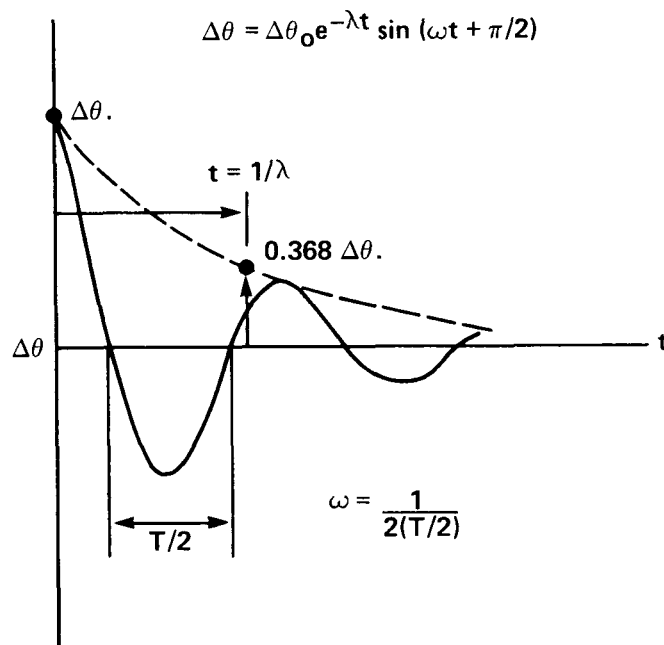


Figure 13.- Graphical technique of determining system frequency and damping from response time-histories.

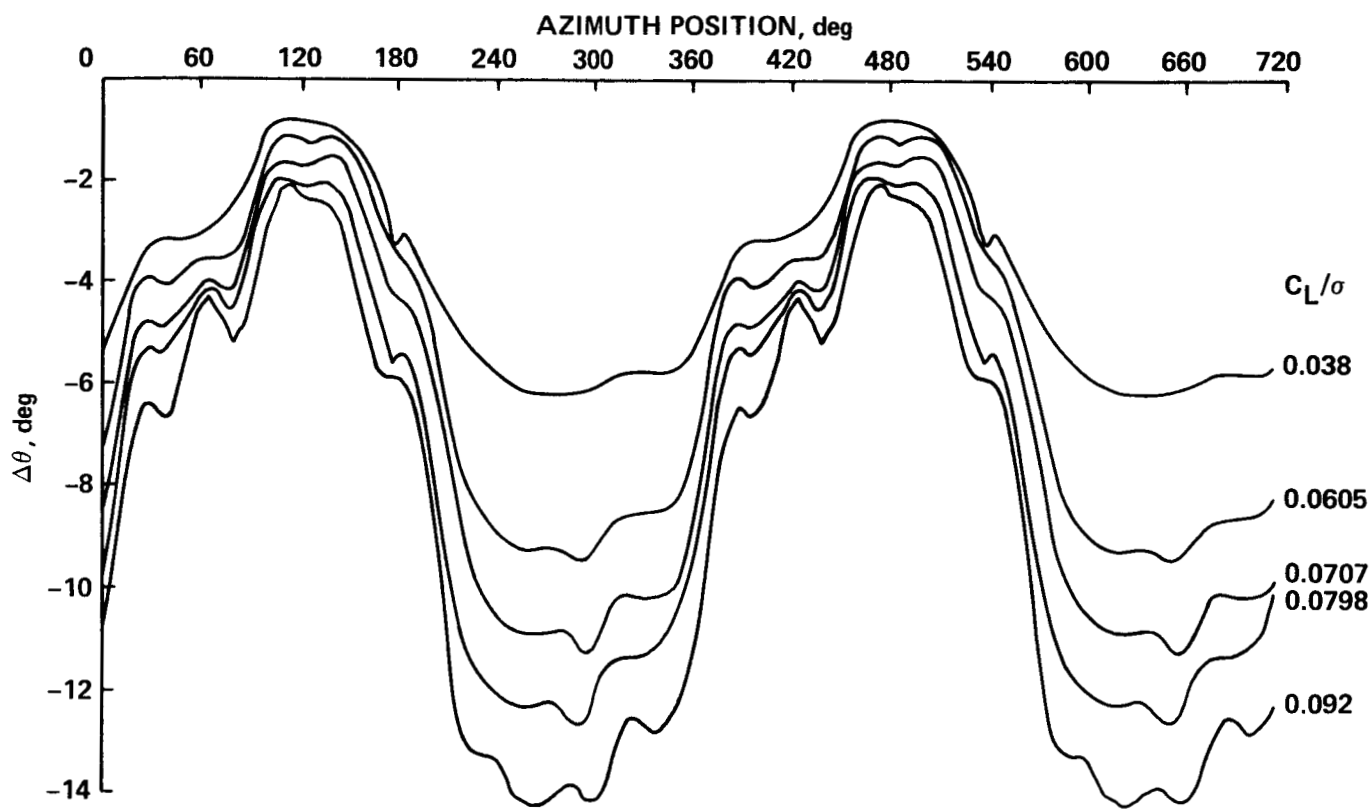
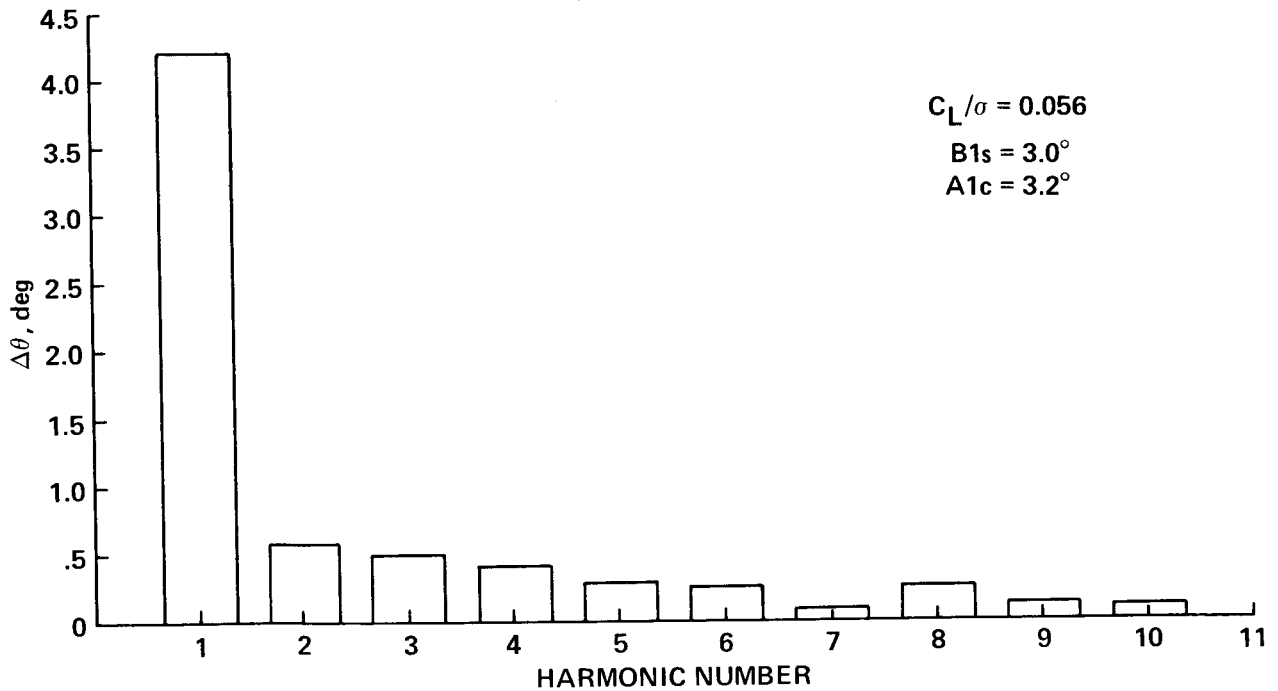
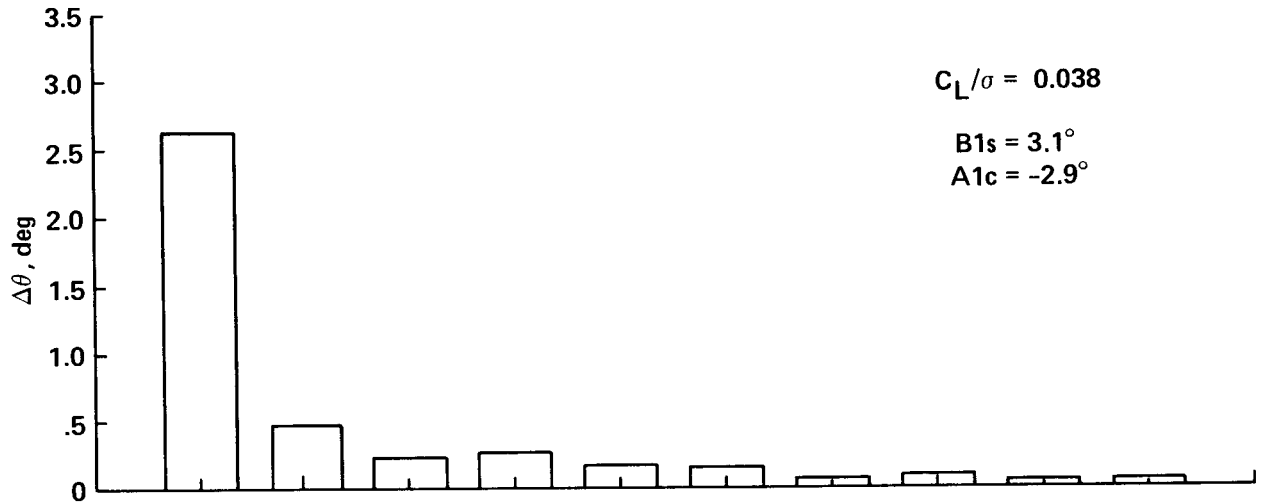
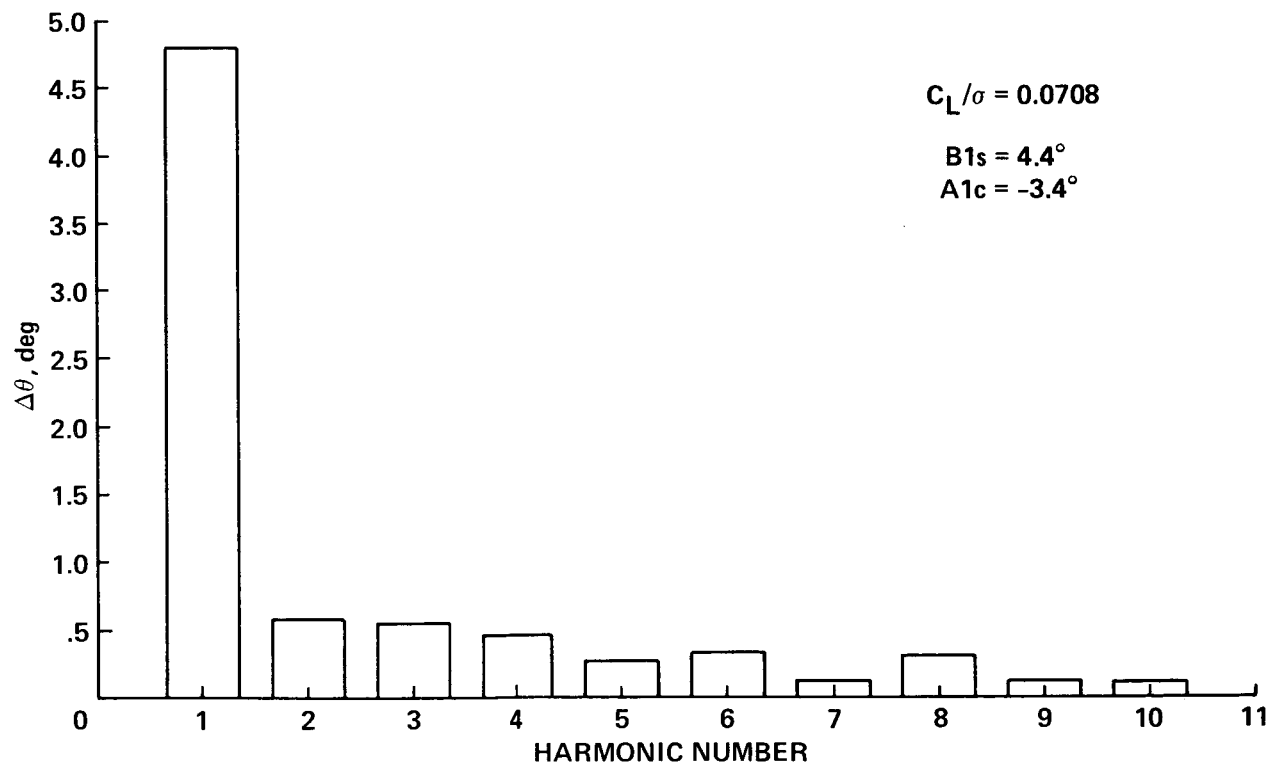
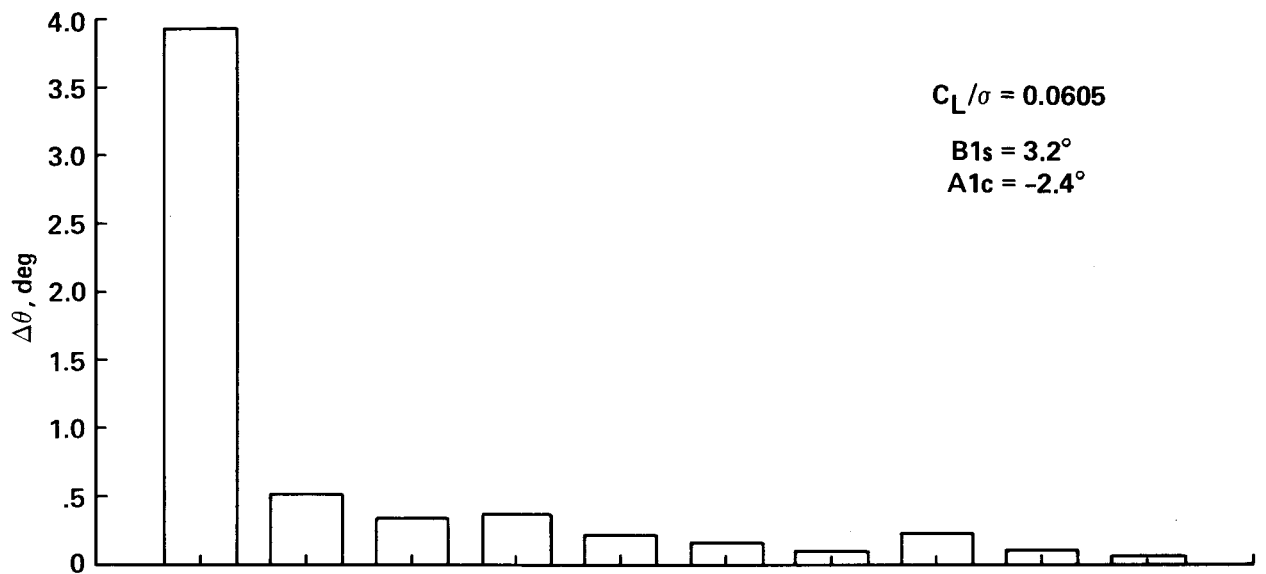


Figure 14.- Variation of free-tip pitch angle differential with rotor lift coefficient: $V/\Omega R = 0.3$ and $\bar{X} = 0.05$.



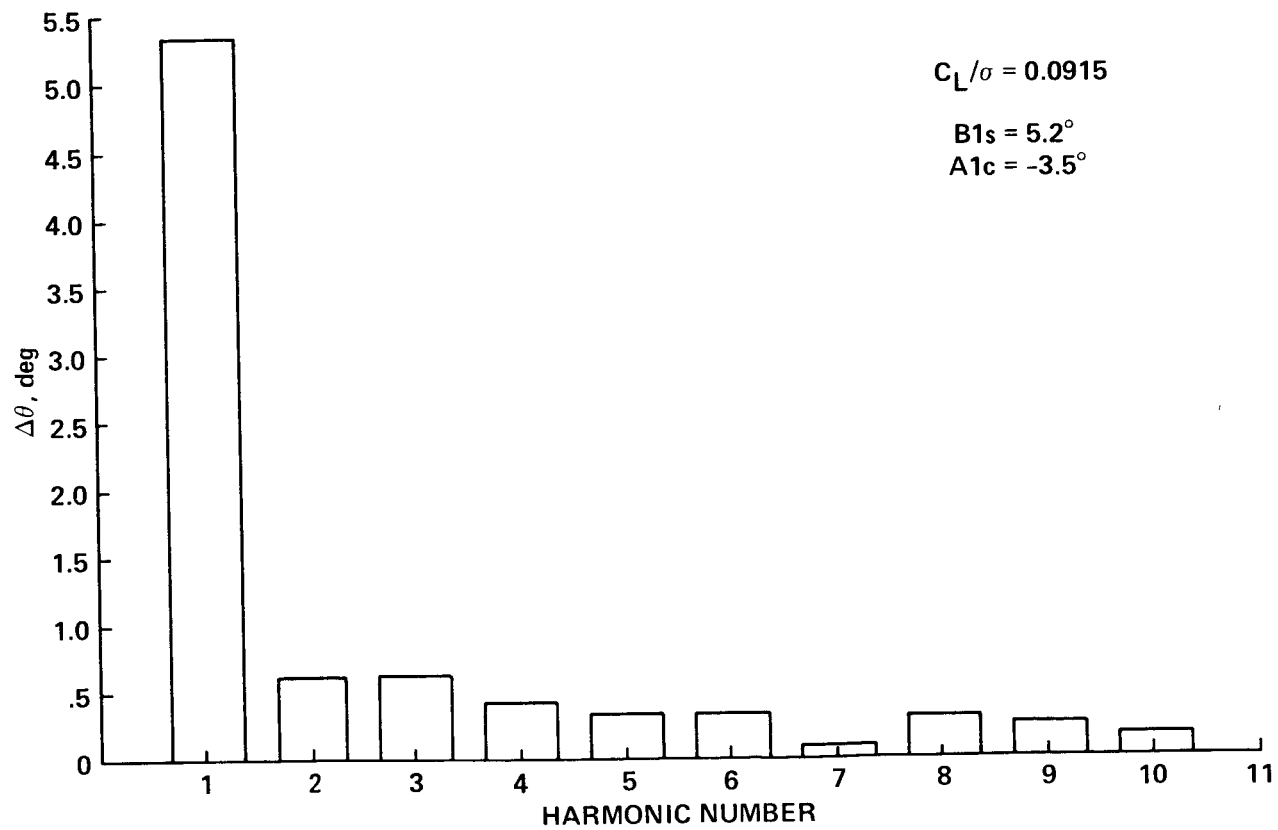
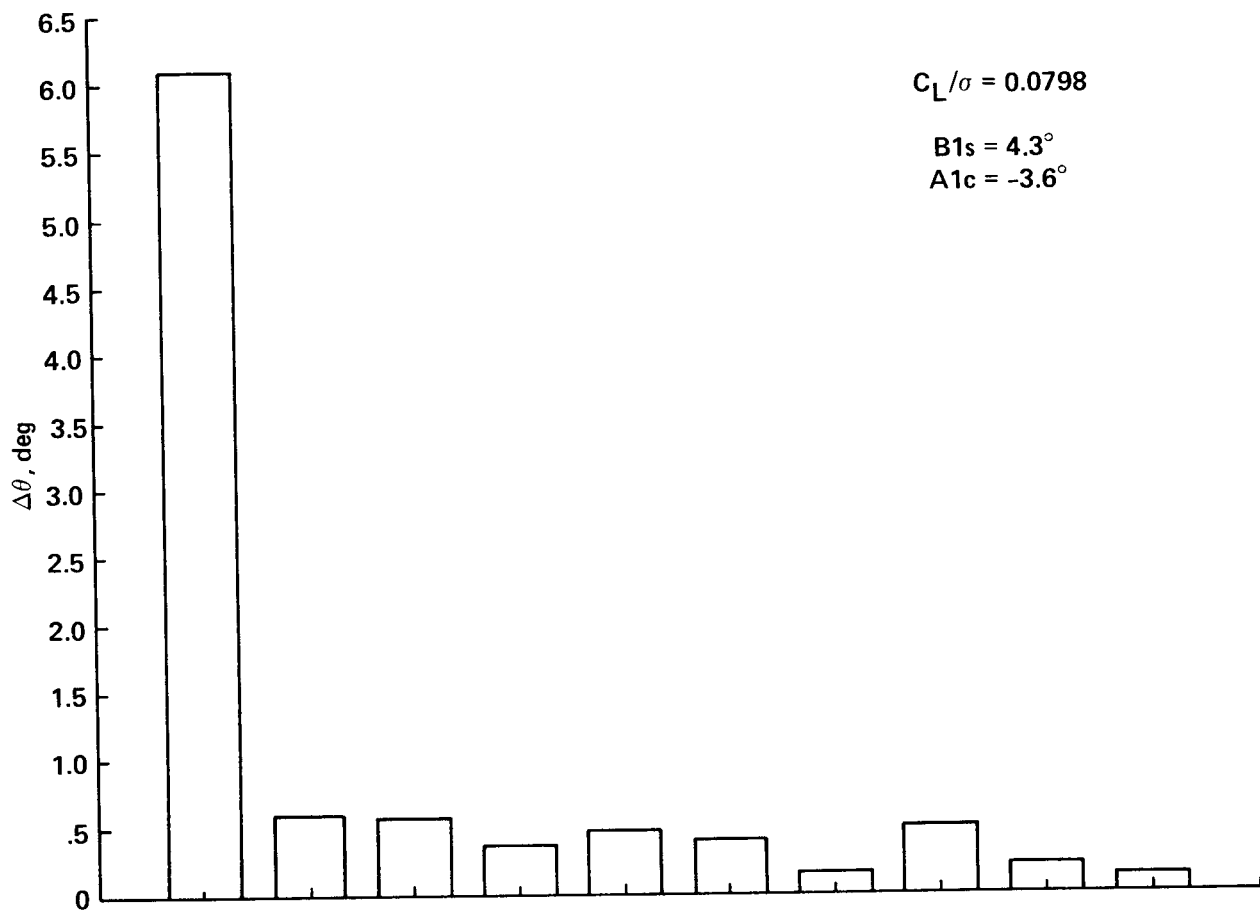
(a) $C_L/\sigma = 0.038$ and 0.056 .

Figure 15.- Harmonic content of $\Delta\theta$ for various rotor lift coefficients.



(b) $C_L/\sigma = 0.0605$ and 0.0708 .

Figure 15.- Continued.



(c) $C_L/\sigma = 0.0798$ and 0.0915 .

Figure 15.- Concluded.

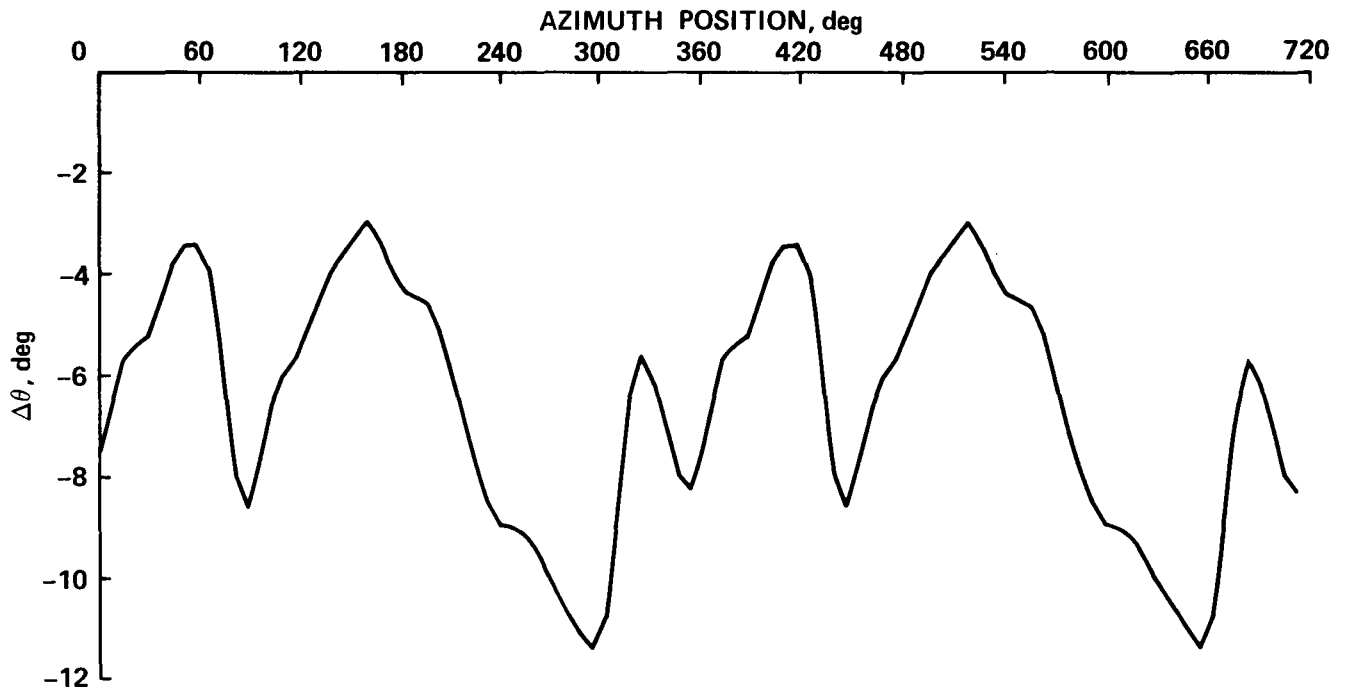
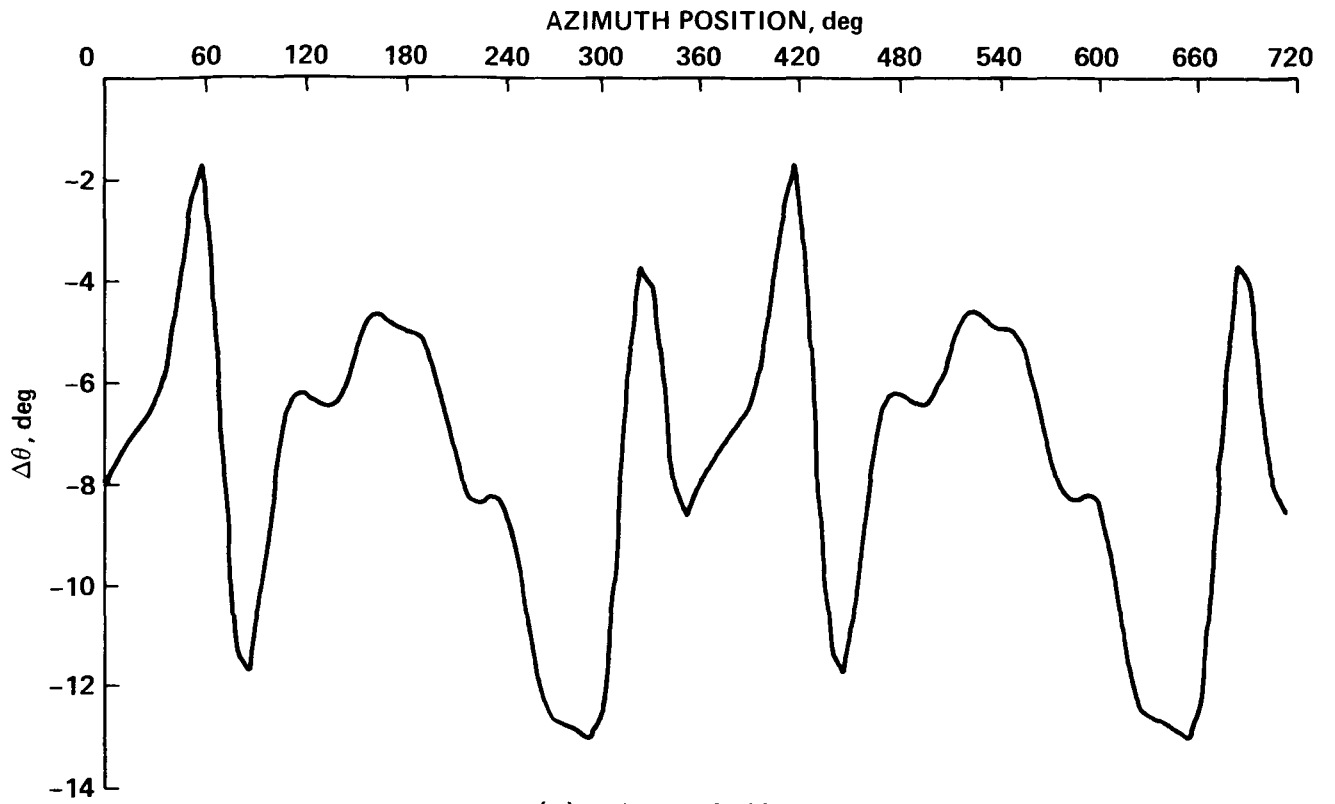


Figure 16.- Variation of free-tip $\Delta\theta$ with advance ratio: $C_L/\sigma = 0.0708$, $\bar{X} = 0.05$.

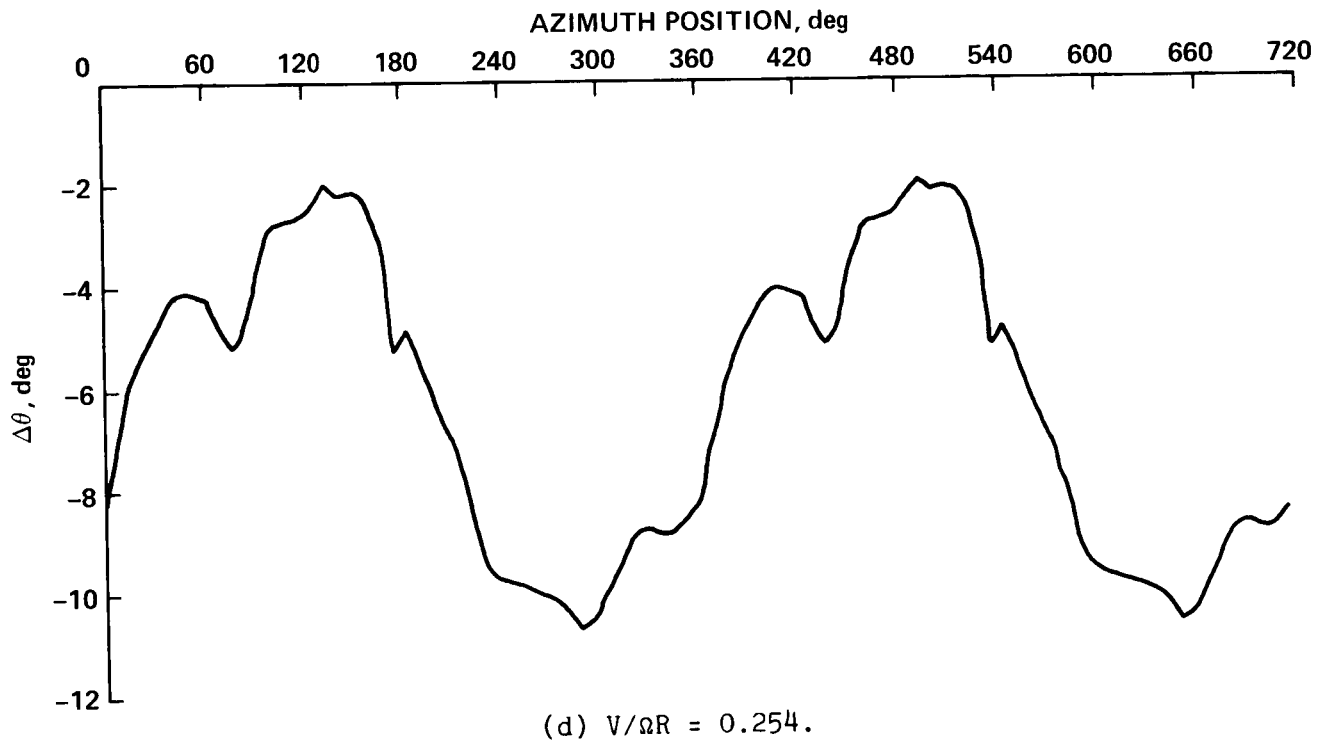
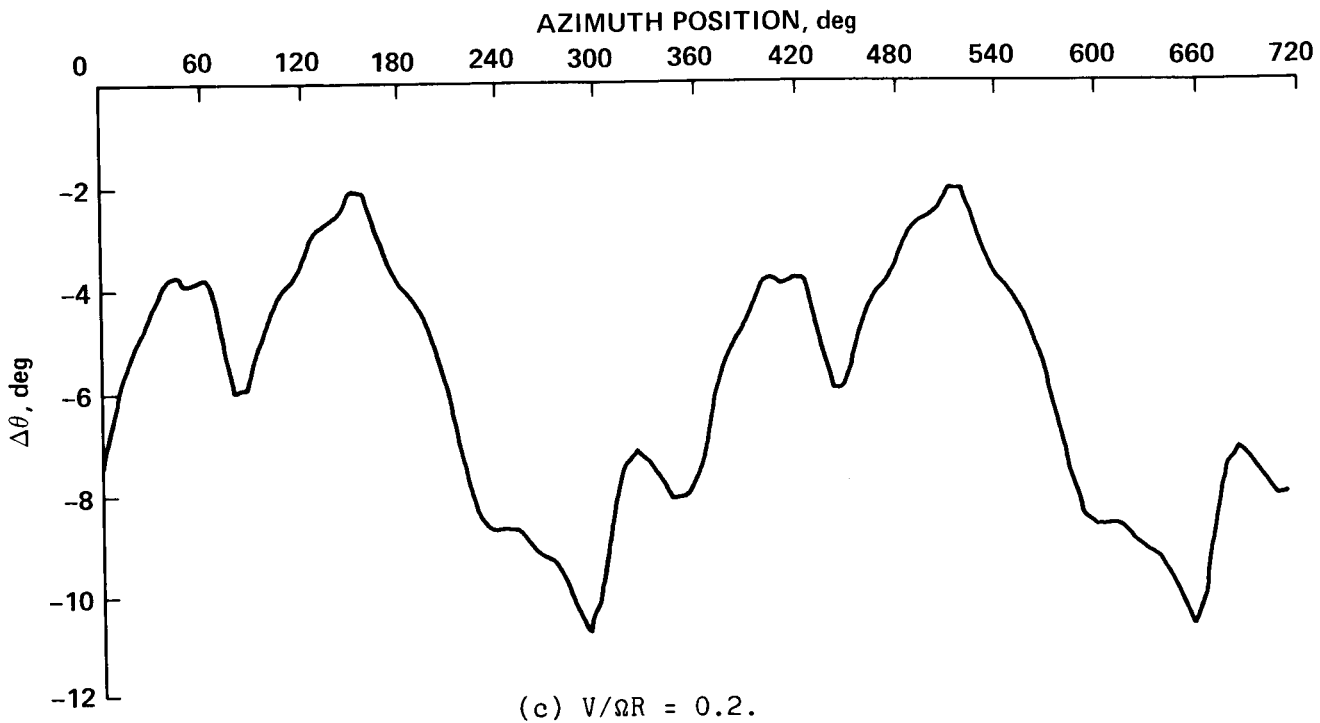
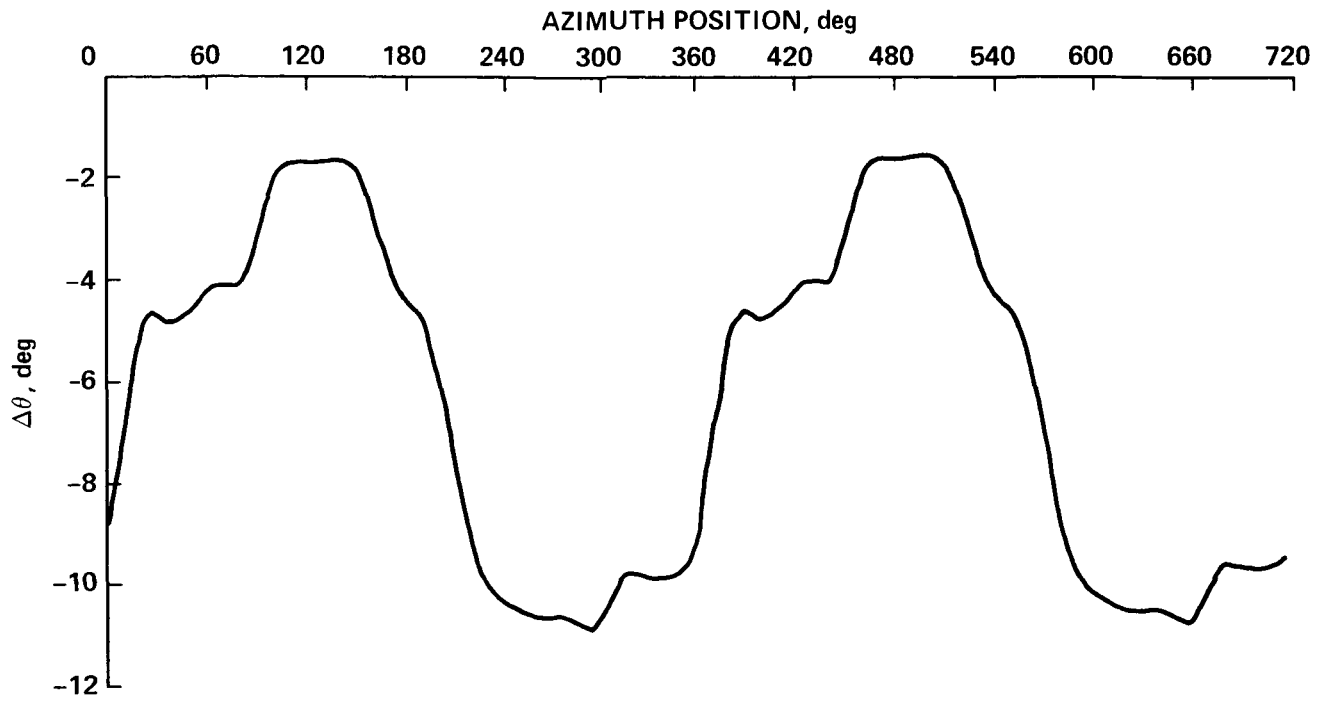
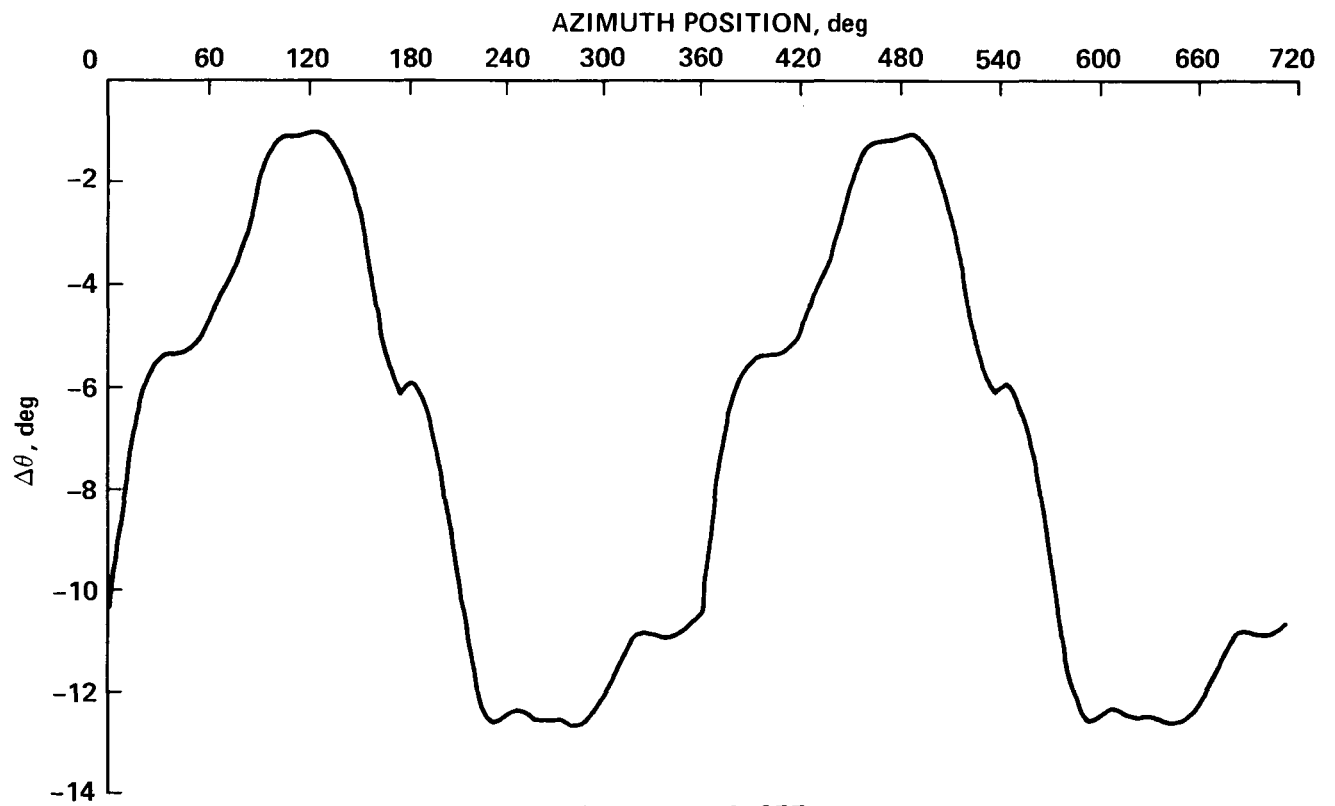


Figure 16.- Continued.

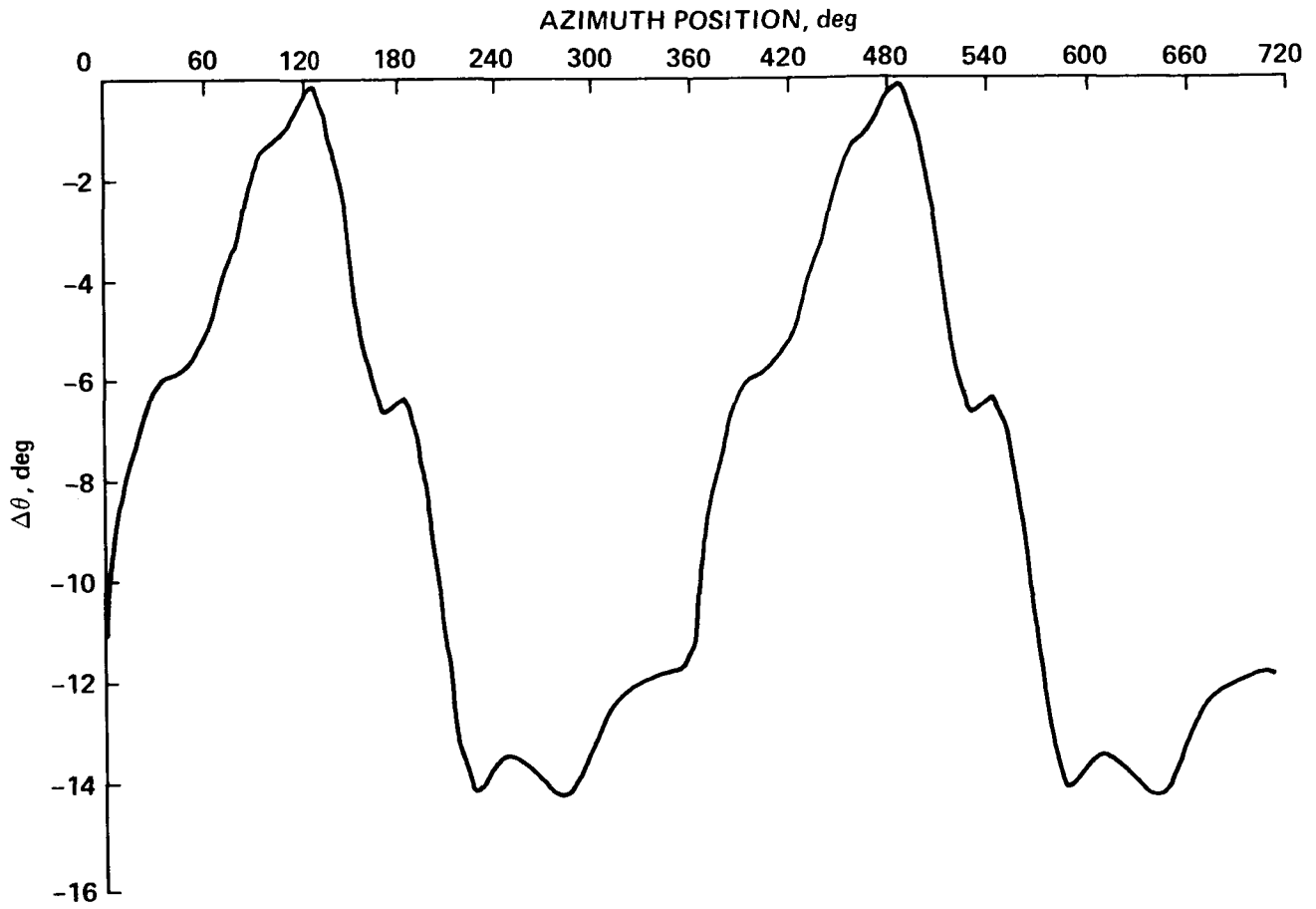


(e) $V/\Omega R = 0.305$.



(f) $V/\Omega R = 0.357$.

Figure 16.- Continued.



(g) $V/\Omega R = 0.391$.

Figure 16.- Concluded.

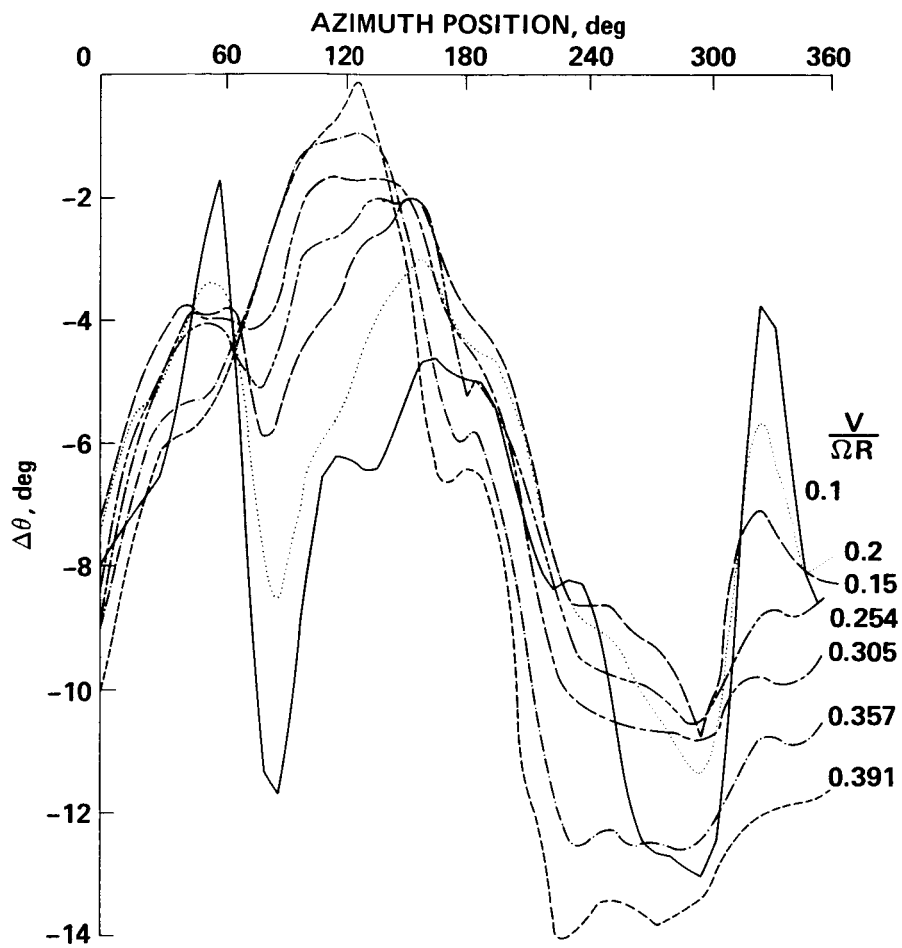
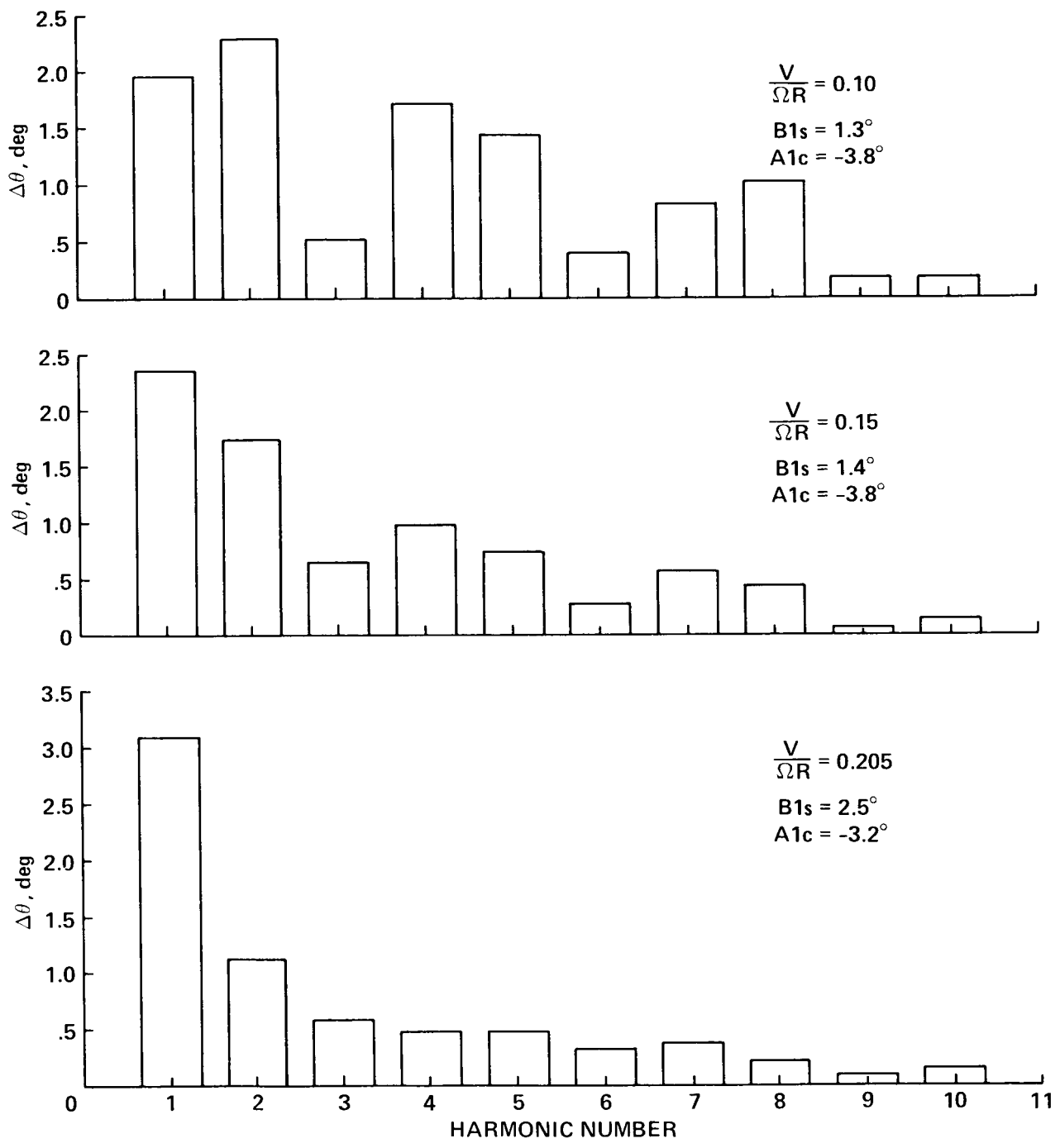
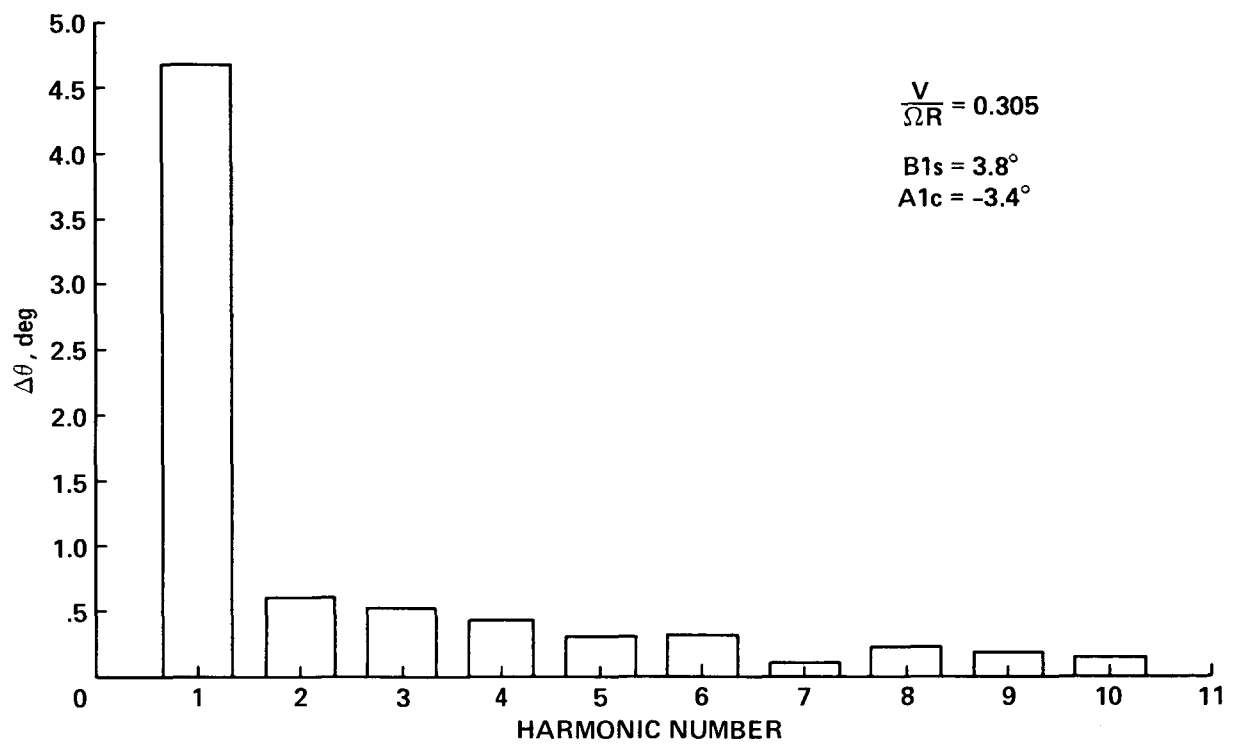
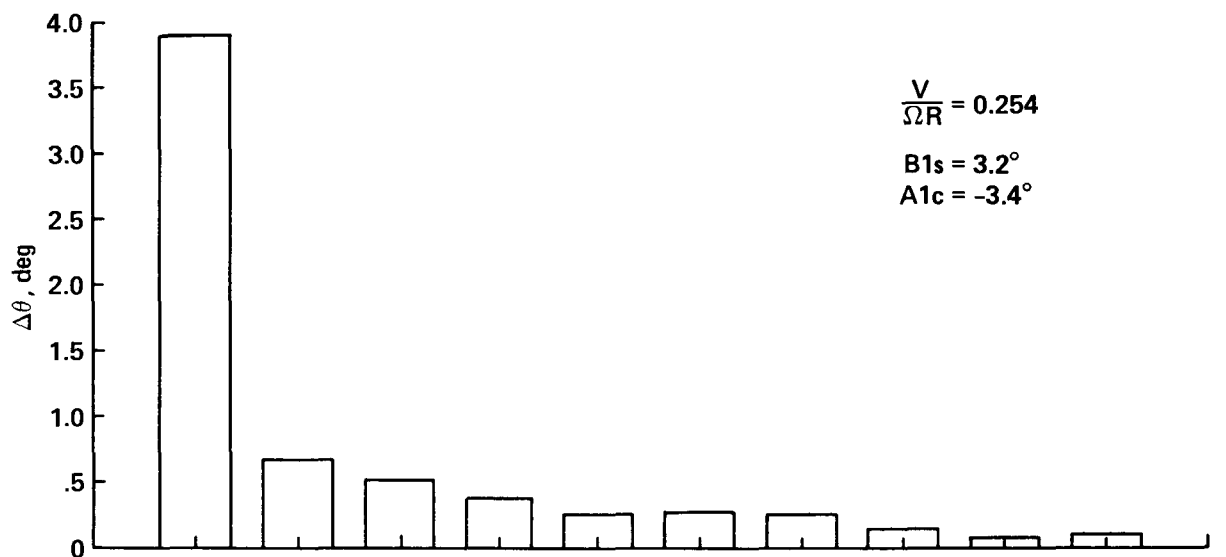


Figure 17.- Compilation of free-tip $\Delta\theta$ with advance ratio: $C_L/\sigma = 0.0708$,
 $\bar{X} = 0.05$.



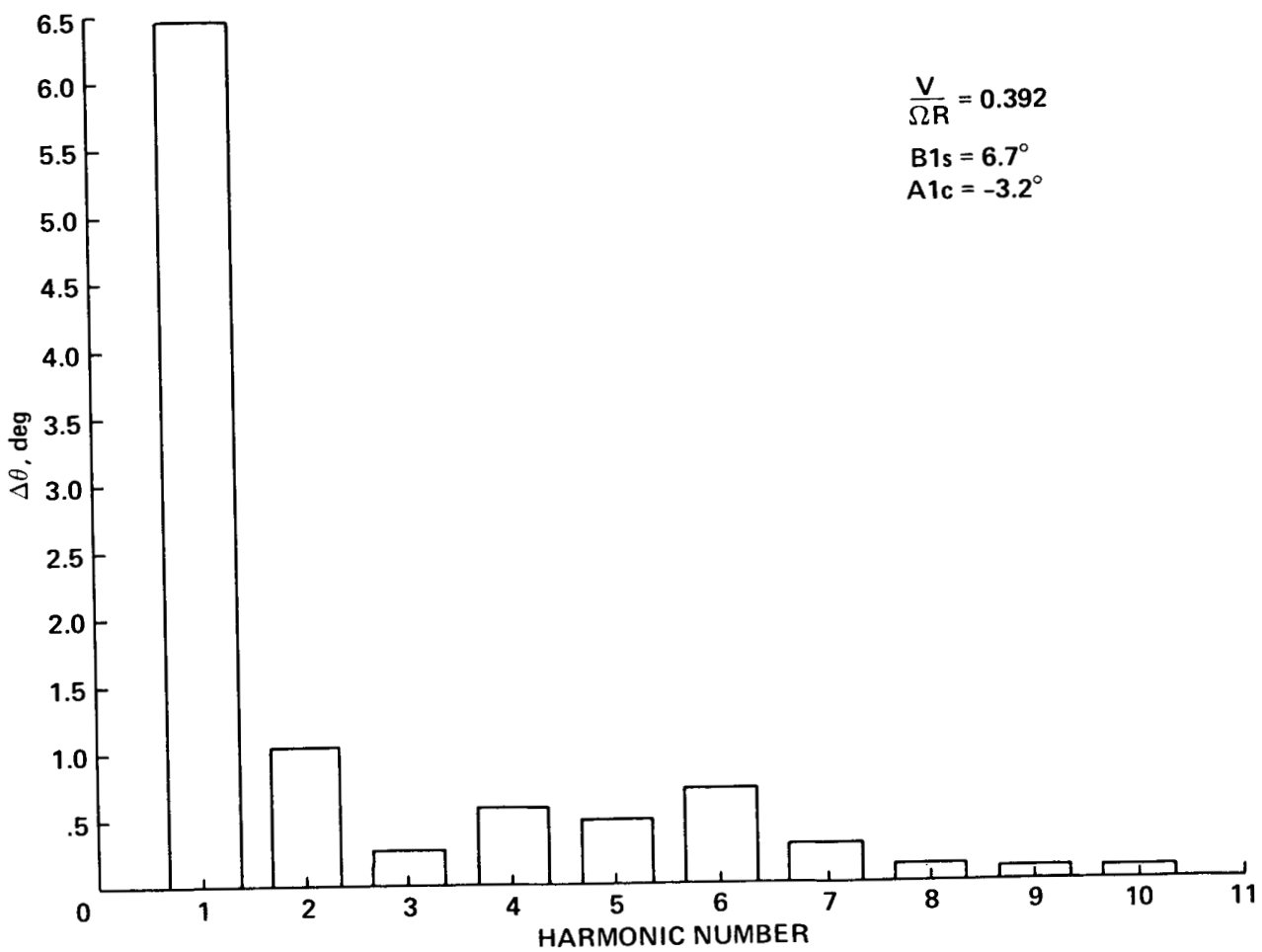
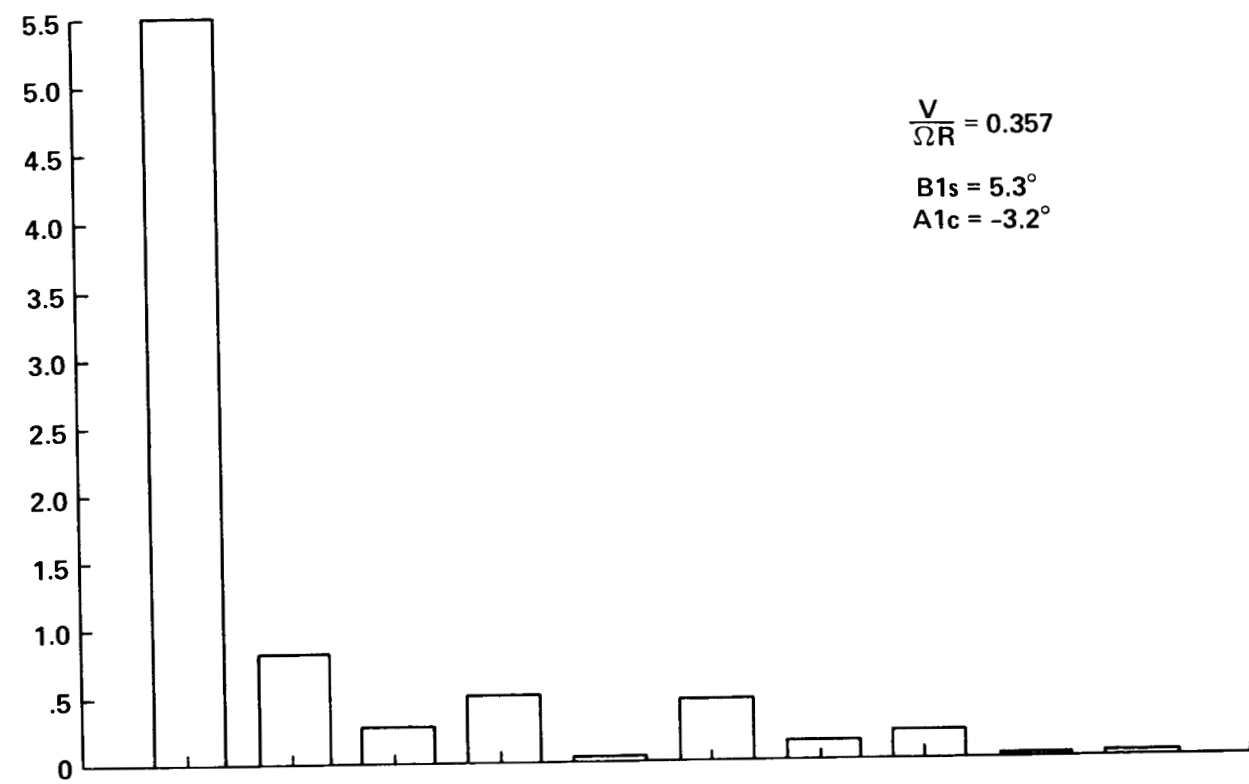
(a) $V/\Omega R = 0.10, 0.15, \text{ and } 0.205.$

Figure 18.- Harmonic content of $\Delta\theta$ at various advance ratios: $C_L/\sigma = 0.0708,$
 $\bar{X} = 0.05.$



(b) $V/\Omega R = 0.254$ and 0.305 .

Figure 18.- Continued.



(c) $V/\Omega R = 0.357$ and 0.392 .

Figure 18.- Concluded.

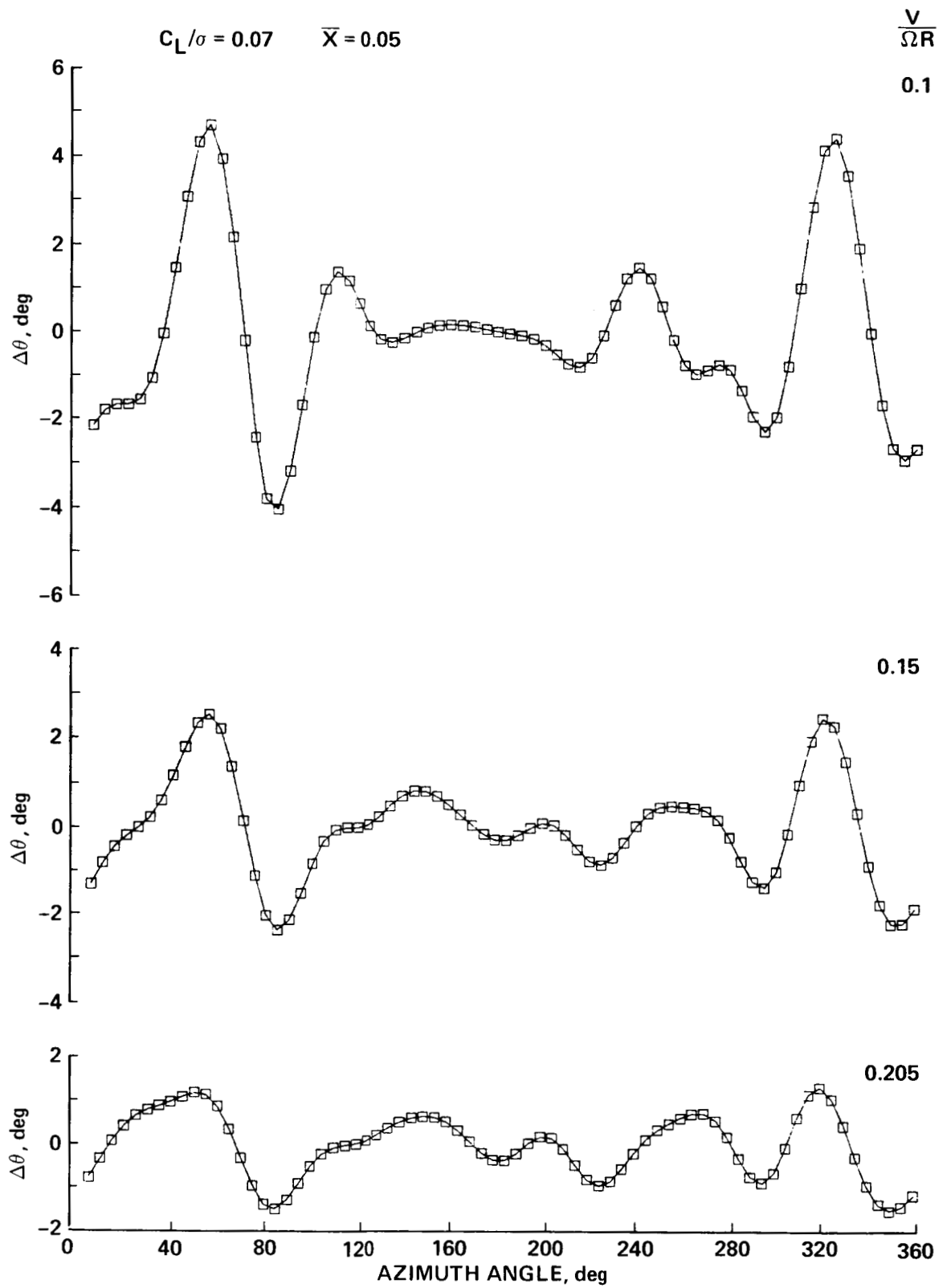


Figure 19.- Recomposition of $\Delta\theta$ waveform from harmonics 3 through 10:
 $V/\Omega R = 0.1$ to 0.2 .

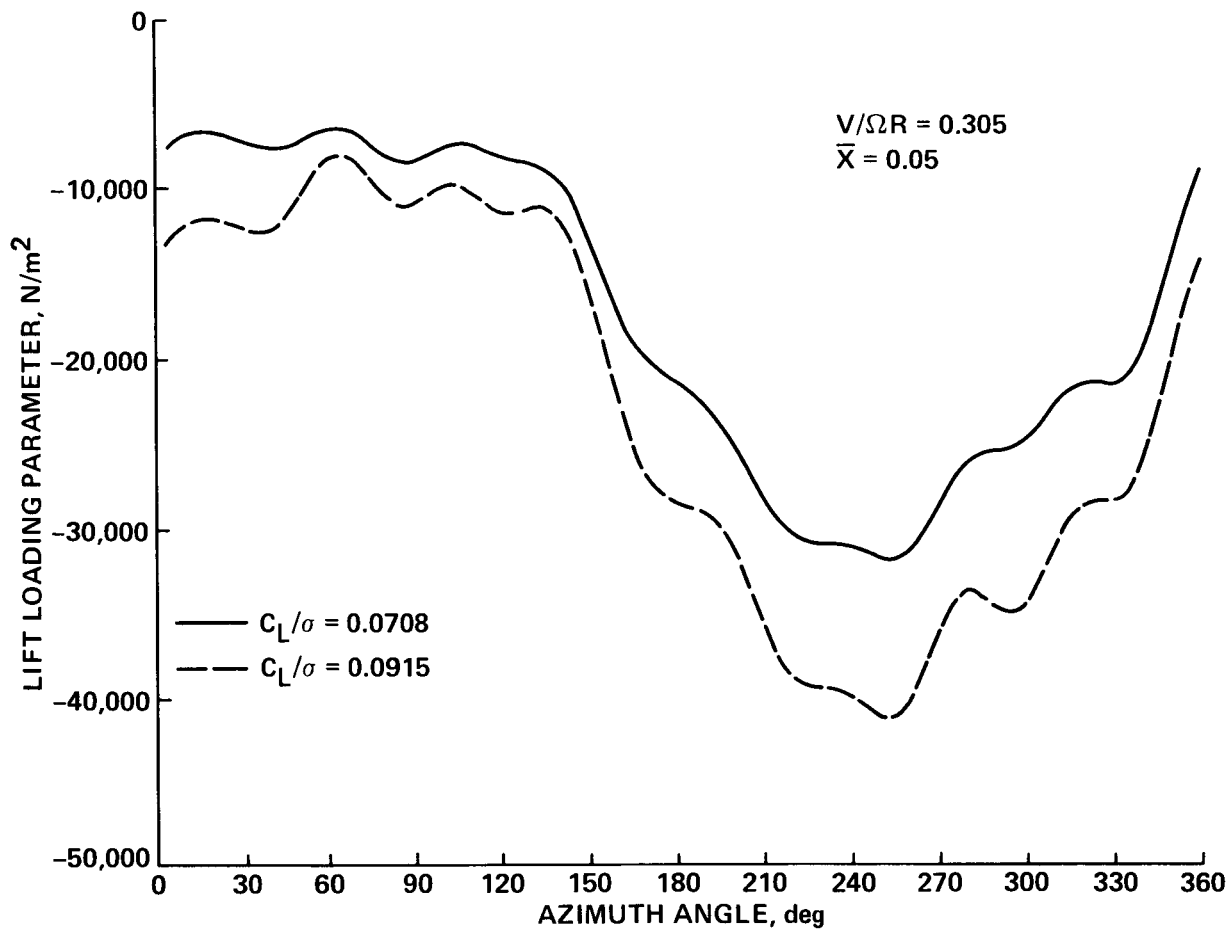


Figure 20.- Azimuthal variation of tip aerodynamic loading parameters utilizing all harmonics: $\bar{X} = 0.05$, $V/\Omega R = 0.305$.

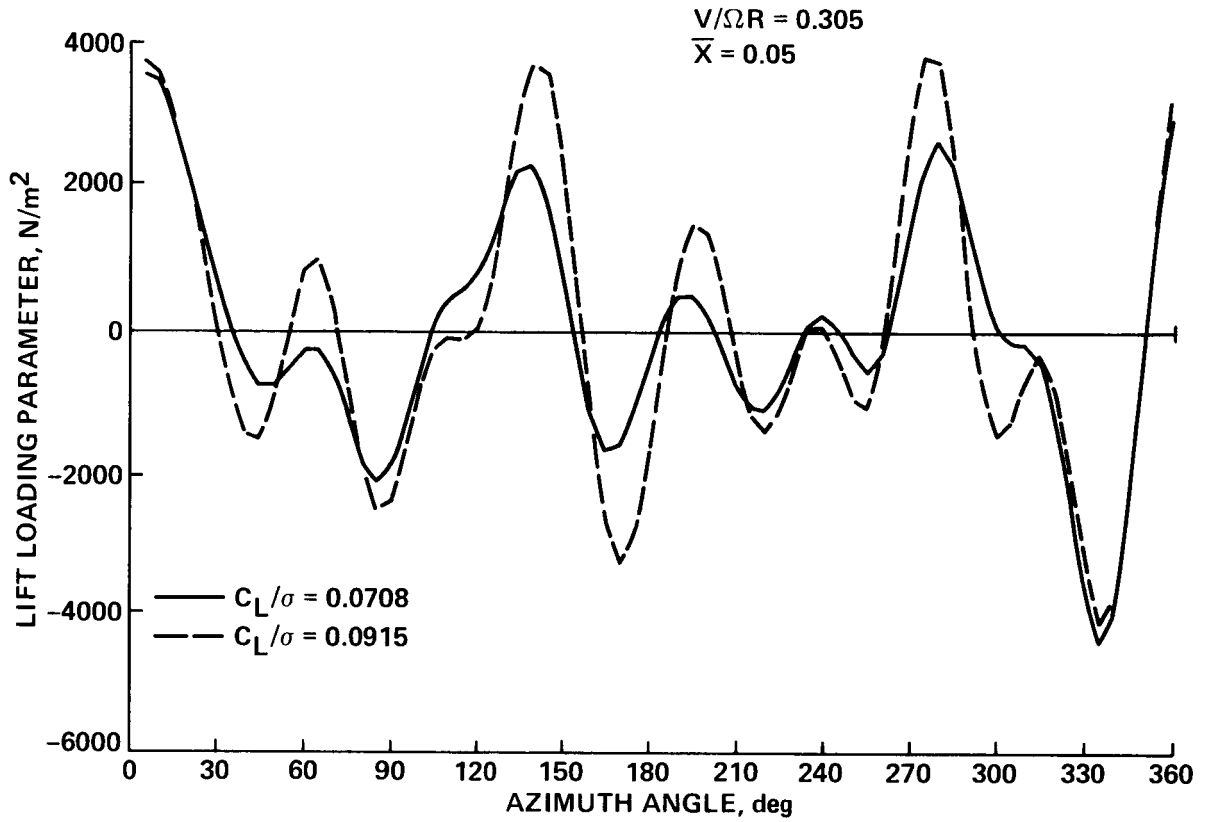


Figure 21.- Aerodynamic loading parameter utilizing harmonics 3 through 10:
 $\bar{X} = 0.05, V/\Omega R = 0.305.$

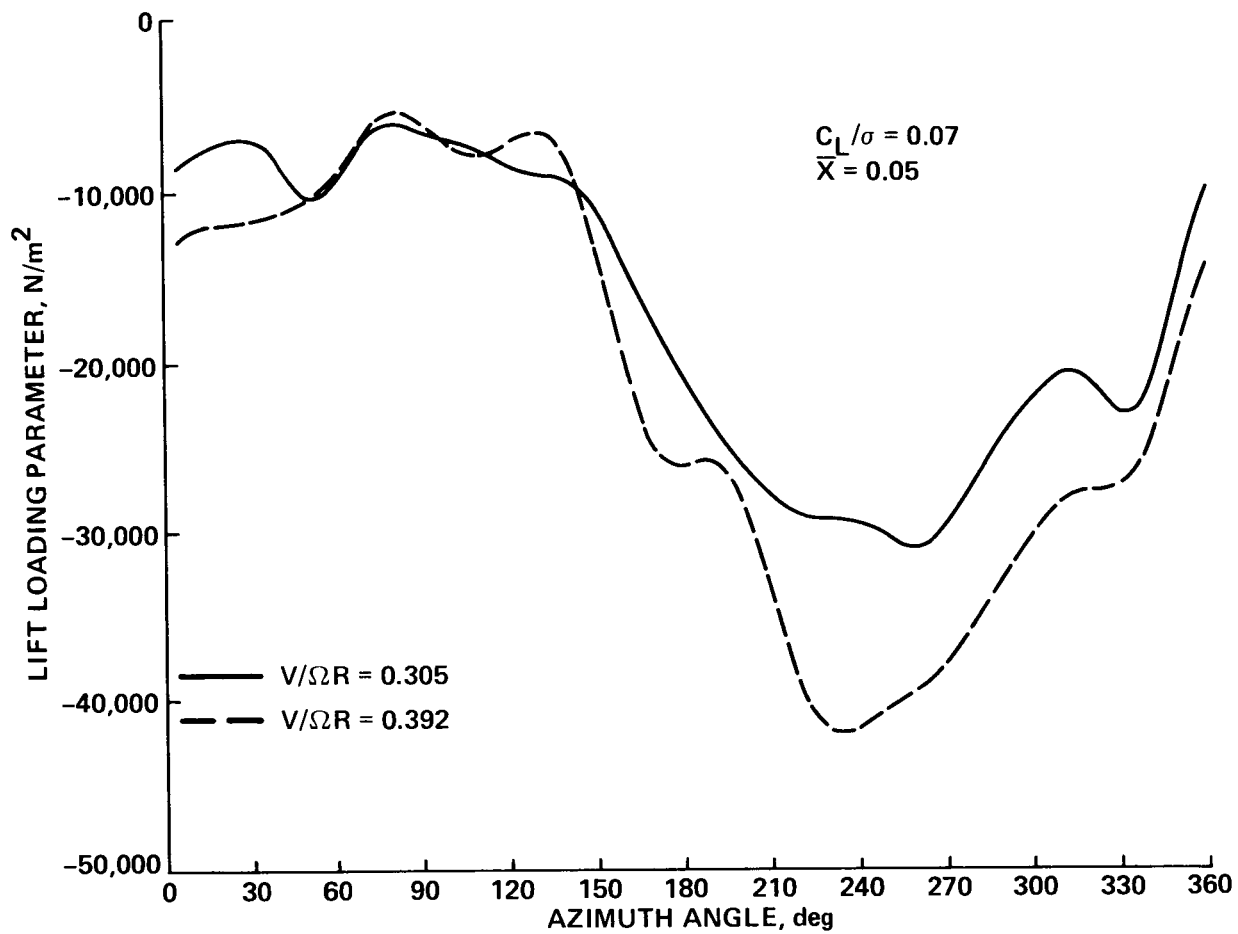


Figure 22.- Azimuthal variation of tip aerodynamic loading parameter with all harmonics: $\bar{X} = 0.05$, $C_L/\sigma = 0.0708$.

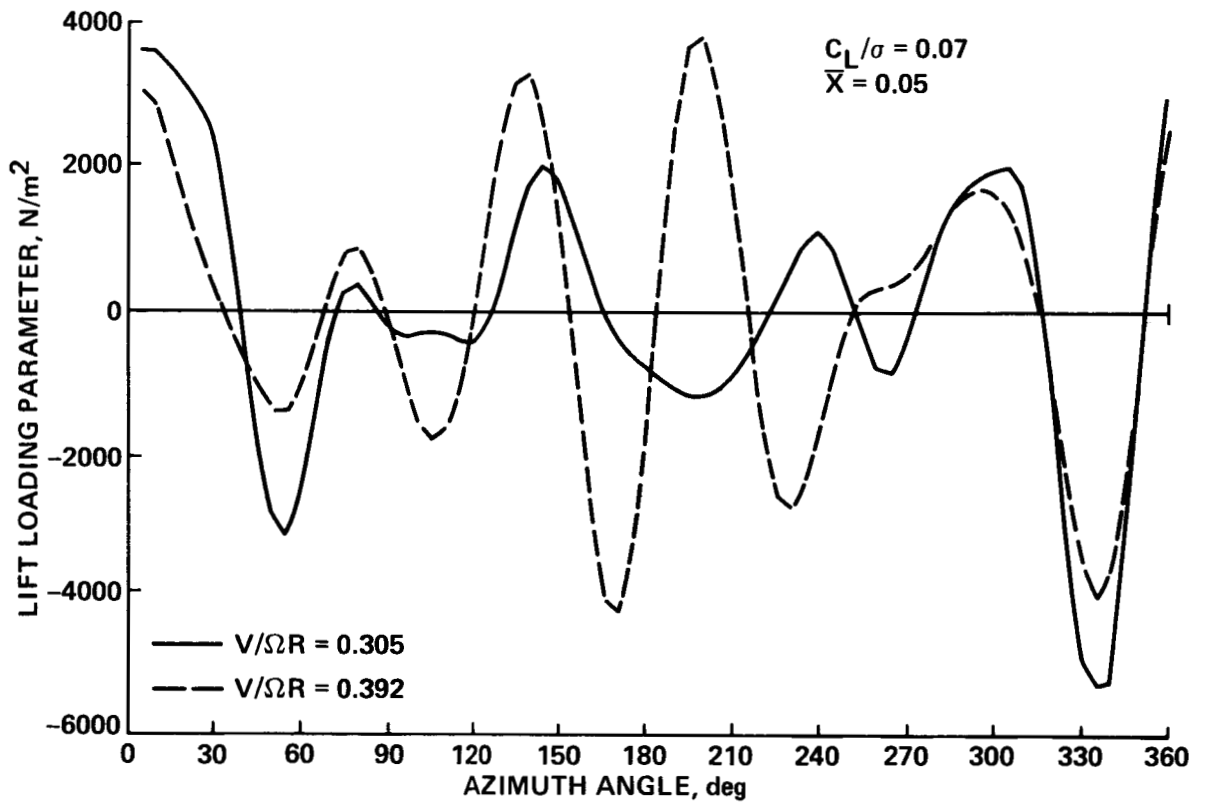


Figure 23.- Aerodynamic loading parameter using only harmonics 3 through 10:
 $\bar{X} = 0.05$, $C_L/\sigma = 0.0708$.

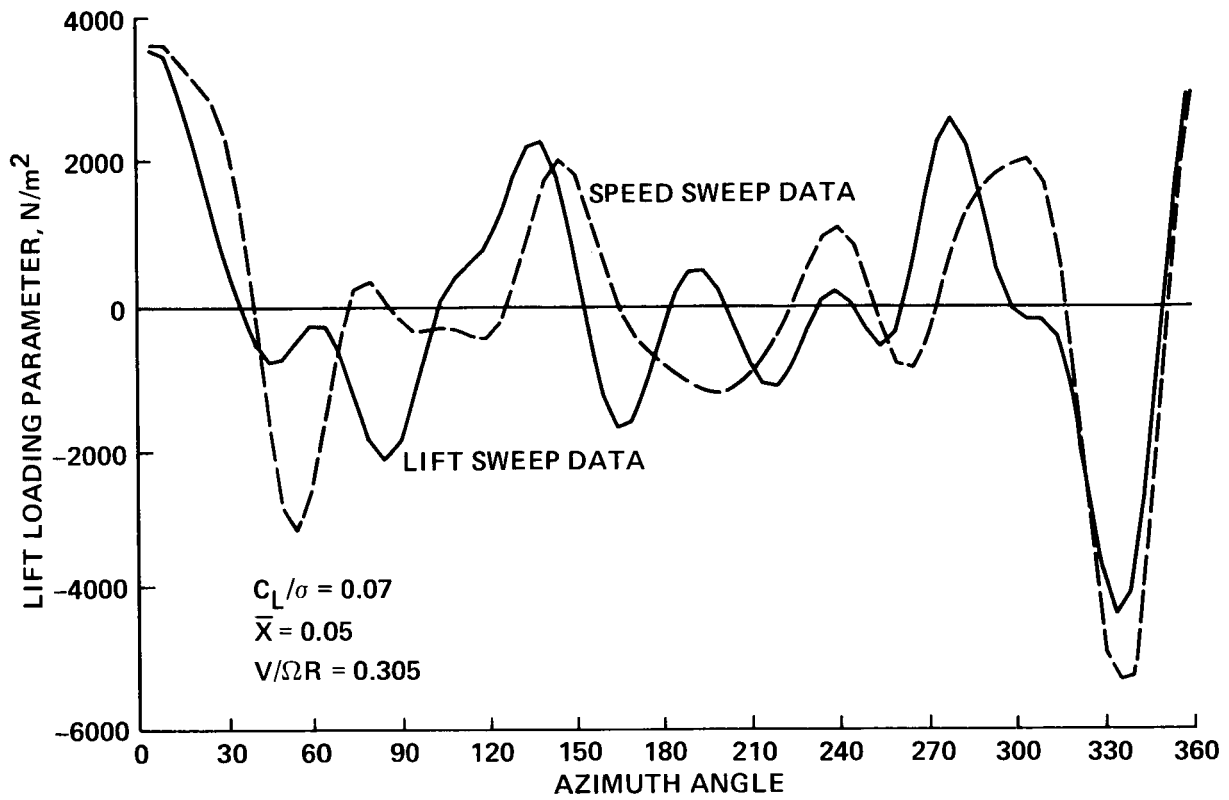


Figure 24.- Comparison of aerodynamic loading parameter: $\bar{X} = 0.05$, $C_L/\sigma = 0.0708$, $V/\Omega R = 0.305$.

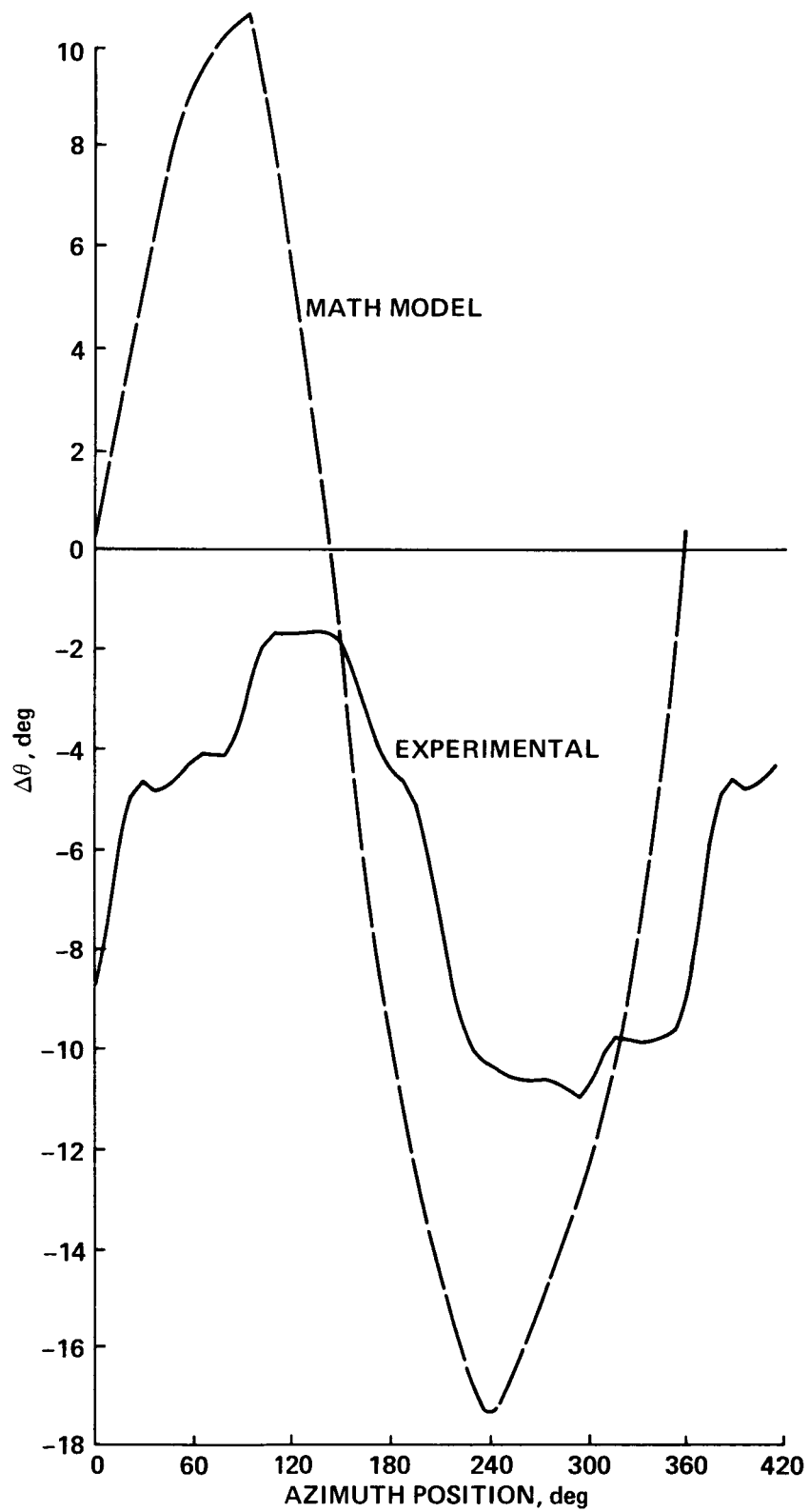


Figure 25.- Comparison of $\Delta\theta$ from wind-tunnel test and from mathematical math model: $C_L/\sigma = 0.0708$, $\bar{X} = 0.05$, $V/\Omega R = 0.305$.

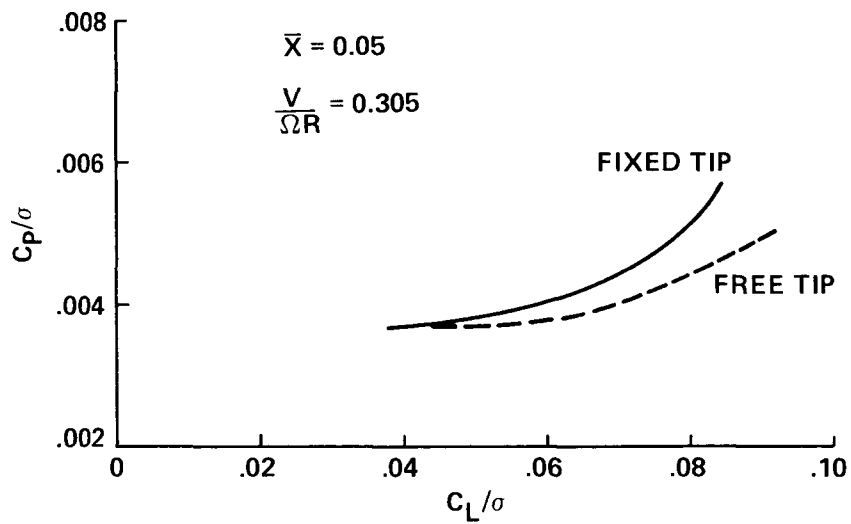


Figure 26.-Comparison of power required by the free-tip rotor and by the fixed-tip rotor at various rotor lift coefficients: $\bar{X} = 0.05$, $V/\Omega R = 0.305$.

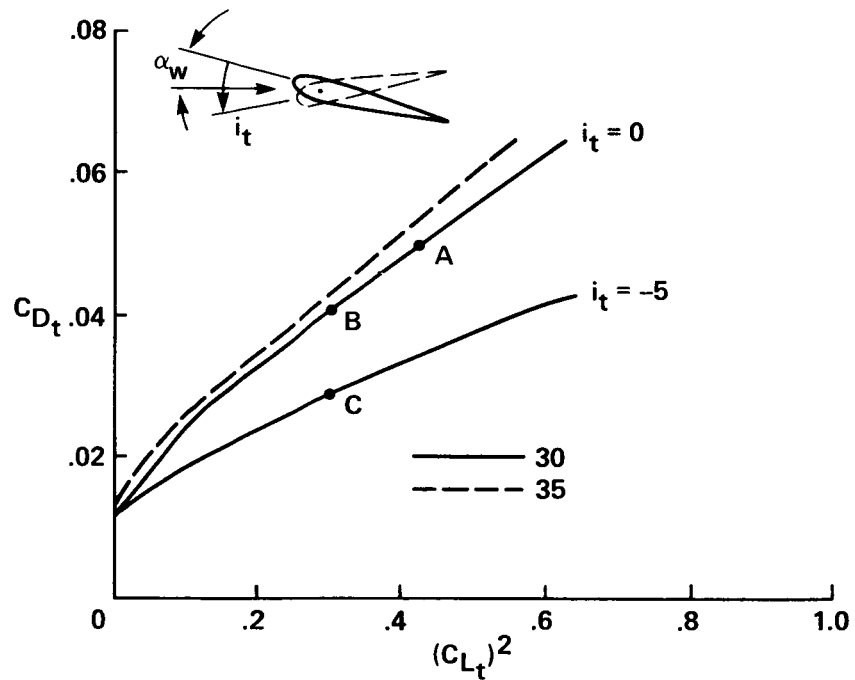
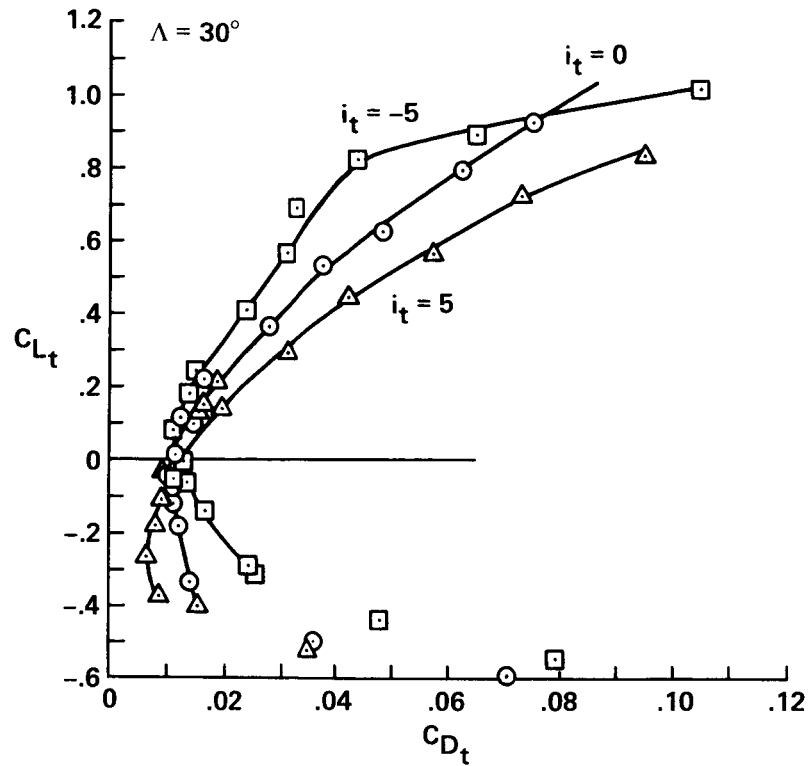


Figure 27.- Aerodynamic drag characteristics of the tip region of a semispan wing at Mach 0.17.

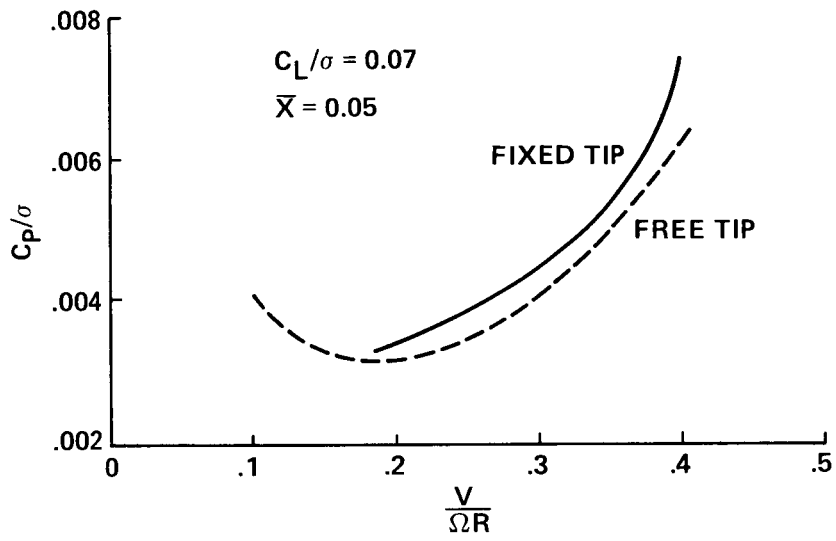


Figure 28.- Speed-power polars for the free- and fixed-tip rotor configurations at $C_L/\sigma = 0.0708$ and $\bar{X} = 0.05$.

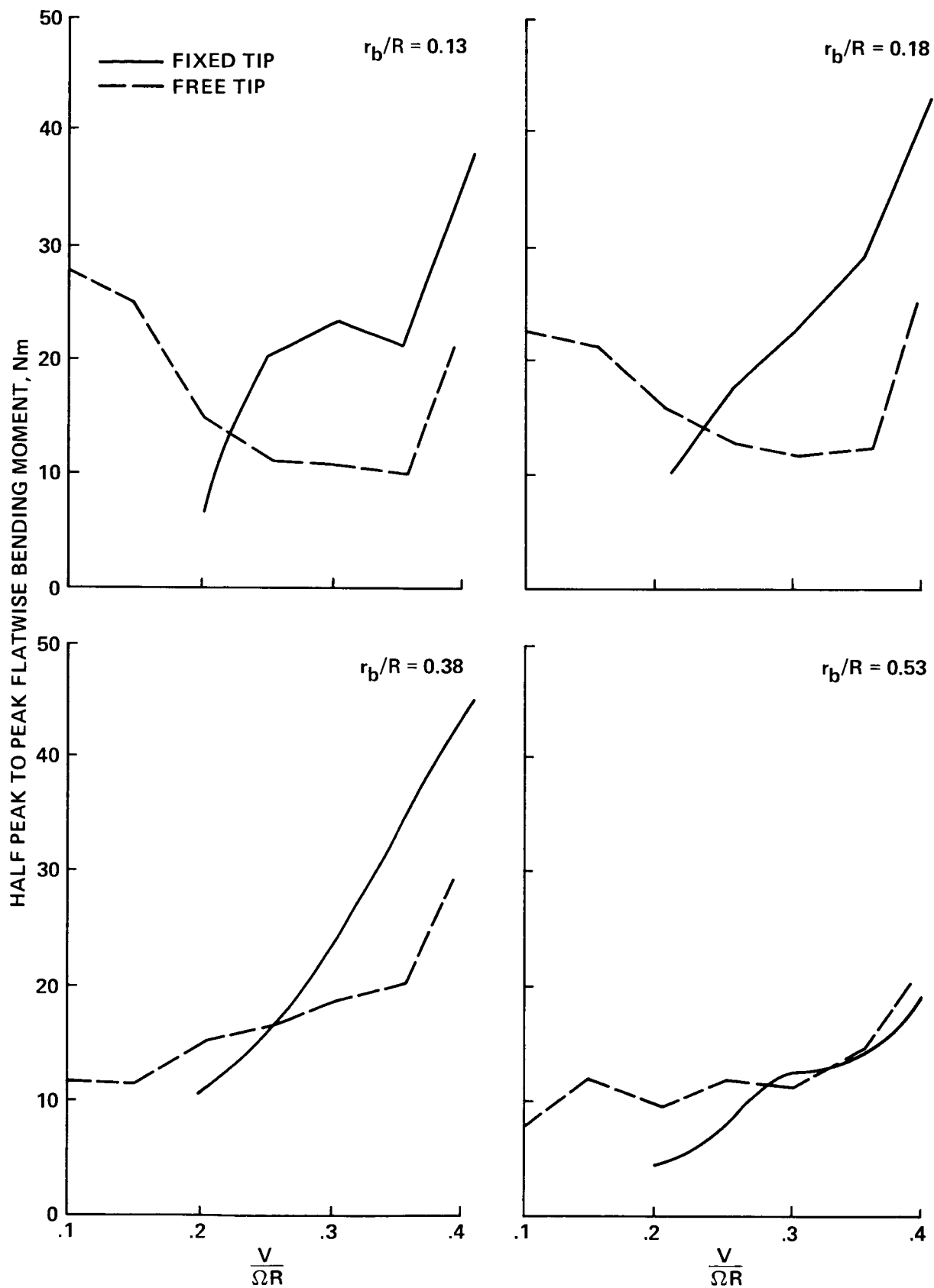


Figure 29.- Half peak-to-peak magnitude of the flatwise bending moments at various blade locations for the free- and fixed-tip configurations: $C_L/\sigma = 0.0708$, $\bar{X} = 0.05$.

ORIGINAL PAGE IS
OF POOR QUALITY

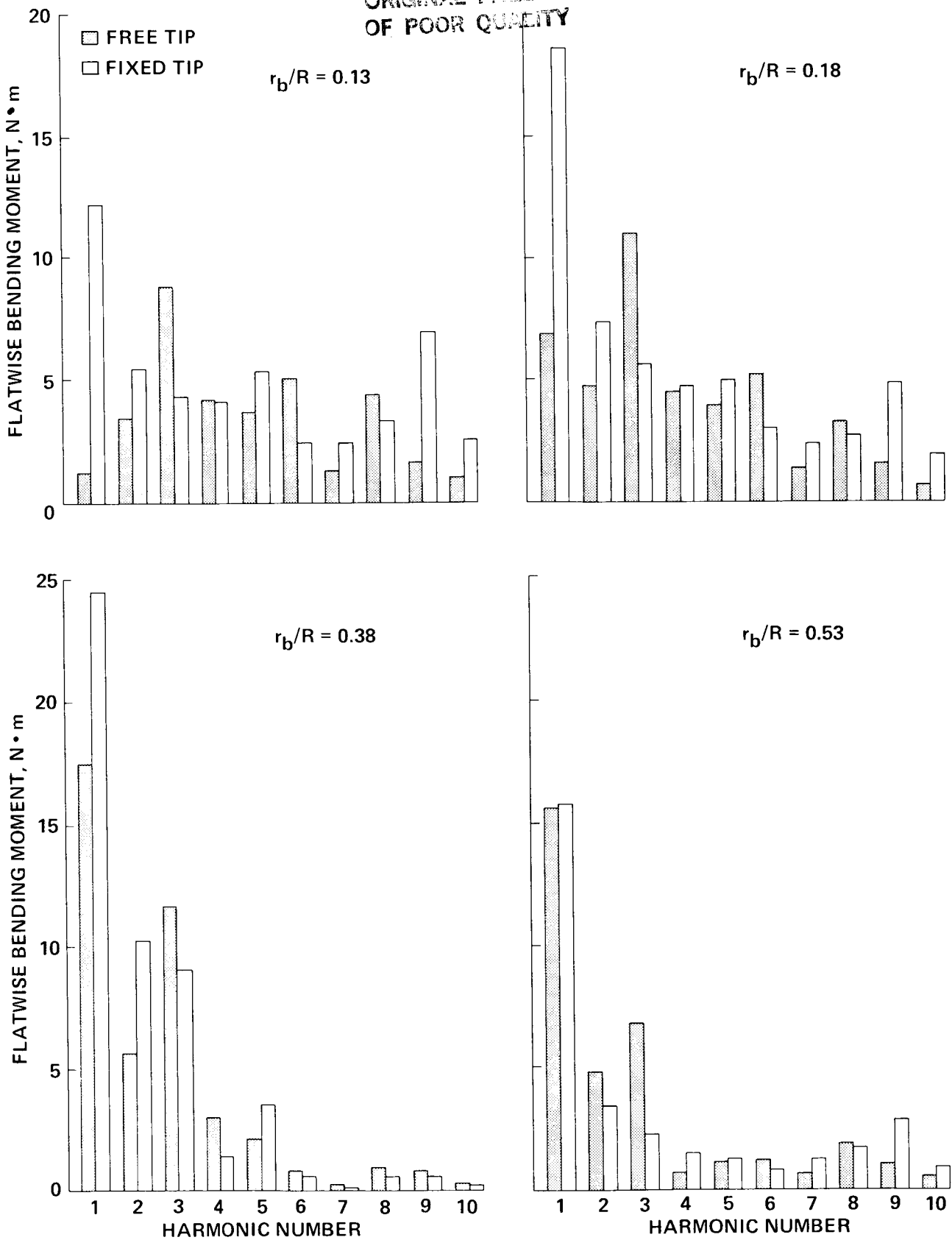


Figure 30.- Comparison of the harmonic content of flatwise bending moments between the free- and fixed-tip configurations: $C_L/\sigma = 0.0708$, $\bar{X} = 0.05$, $V/\Omega R = 0.305$.

ORIGINAL PAGE IS
OF POOR QUALITY

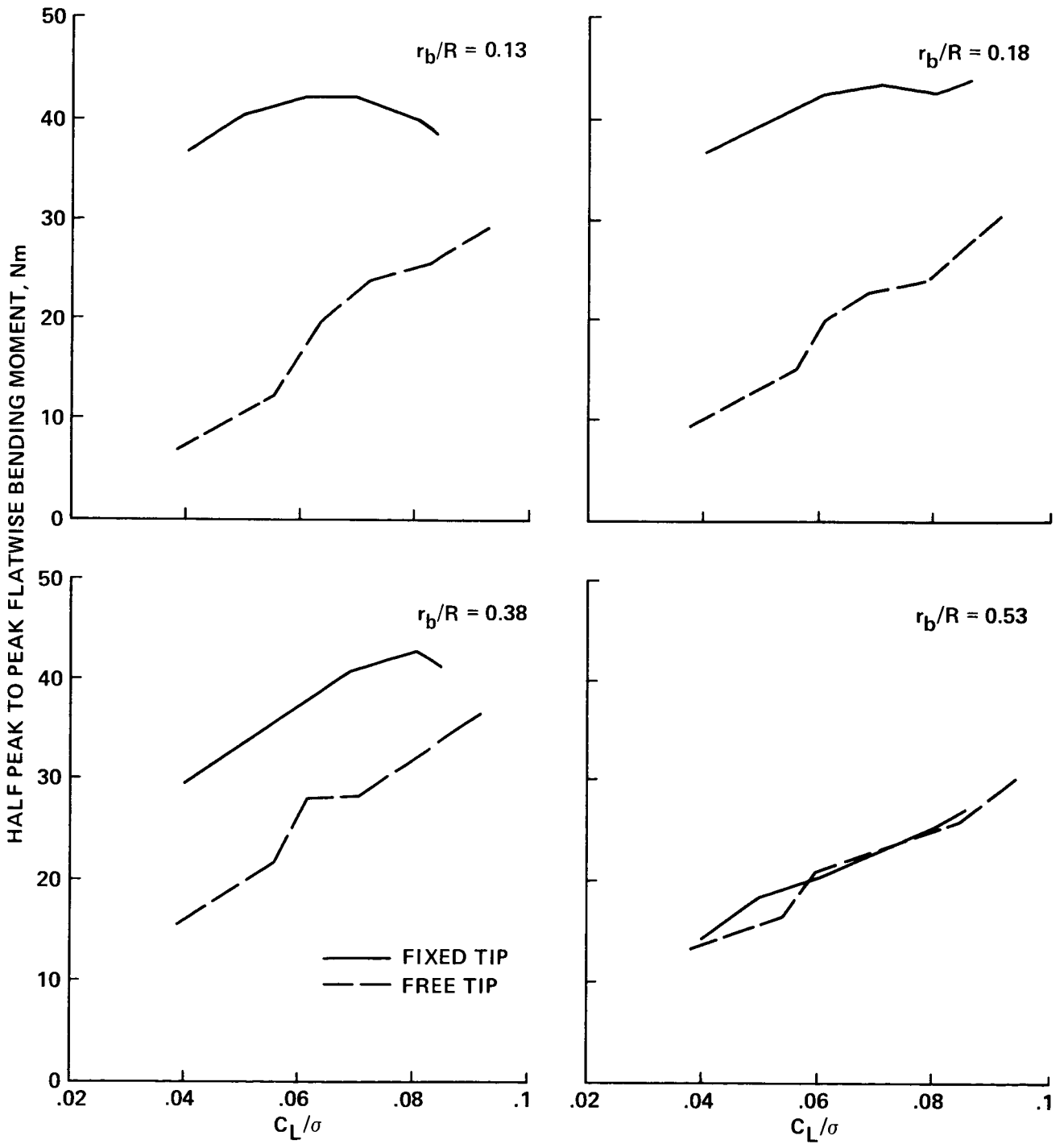


Figure 31.- Variation of the half peak-to-peak magnitudes with rotor lift level:
 $\bar{X} = 0.05, V/\Omega R = 0.305.$

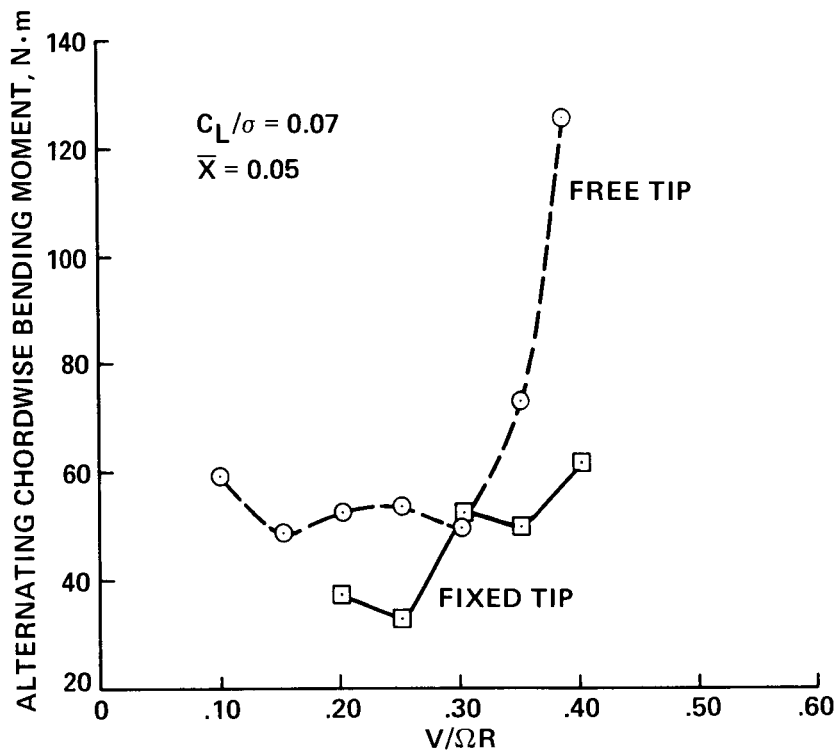


Figure 32.- Comparison of chordwise bending moments between the fixed- and free-tip configurations with advance ratio: $\bar{X} = 0.05$, $C_L/\sigma = 0.0708$.

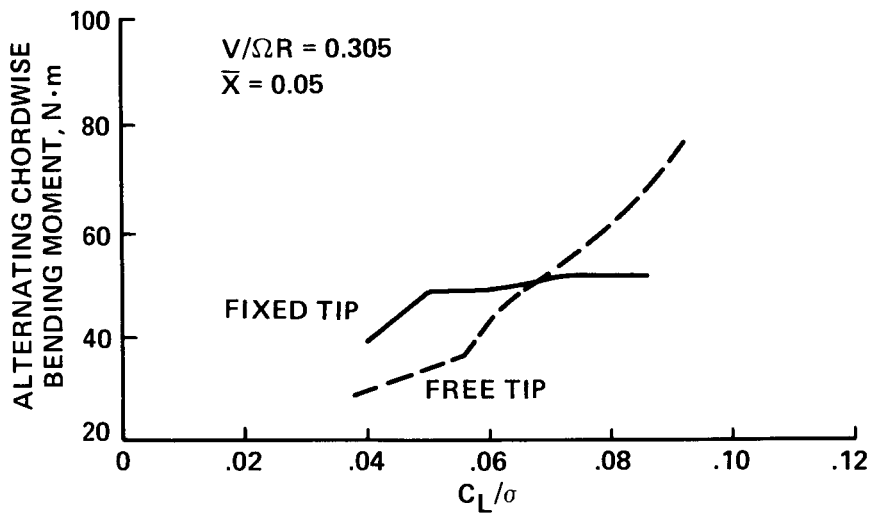


Figure 33.- Comparison of chordwise bending moments at various rotor-lift coefficients: $\bar{X} = 0.05$, $V/\Omega R = 0.305$.

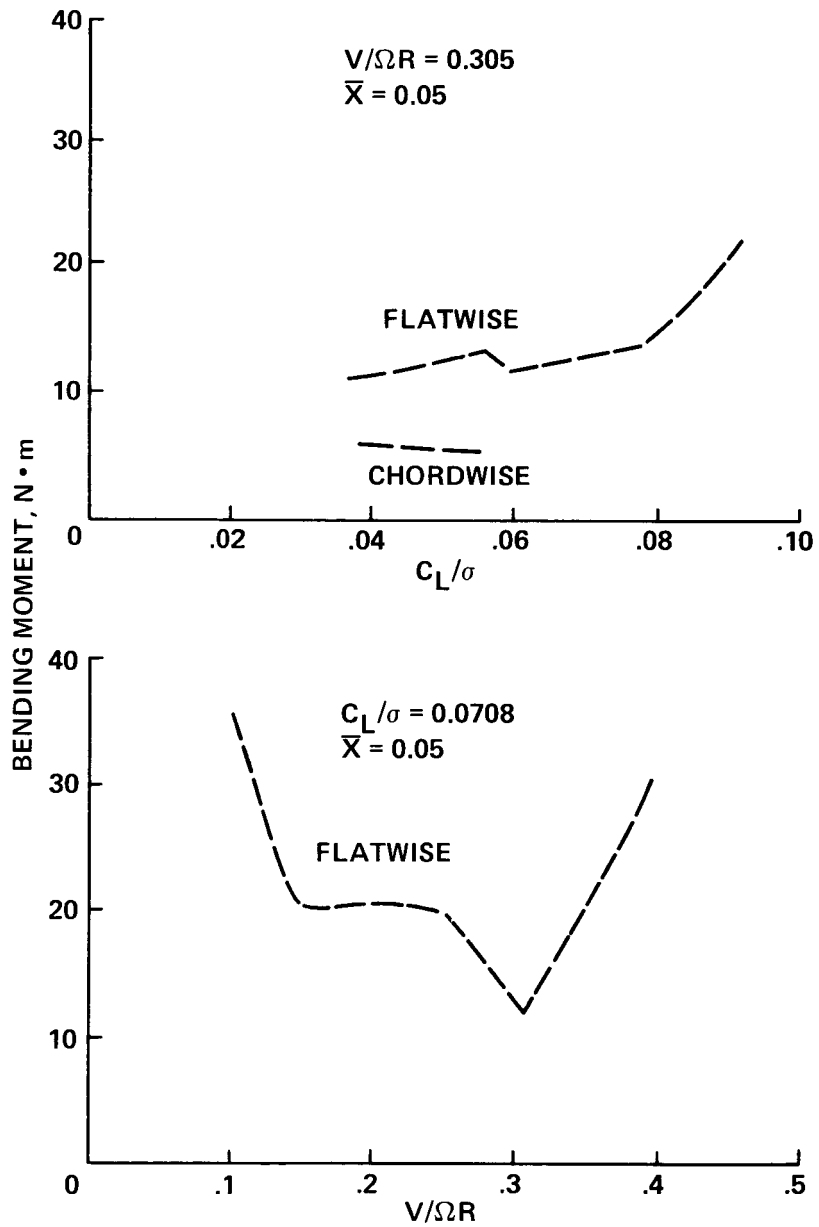


Figure 34.- Half peak-to-peak amplitude of bending moments on the pitch shaft of the free-tip configuration.

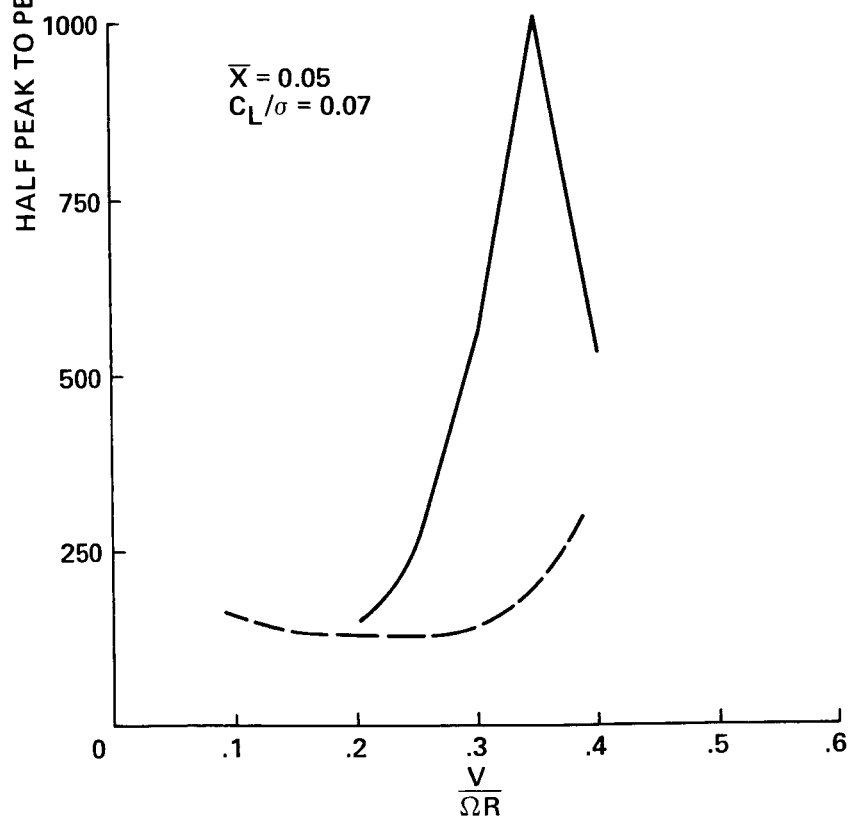
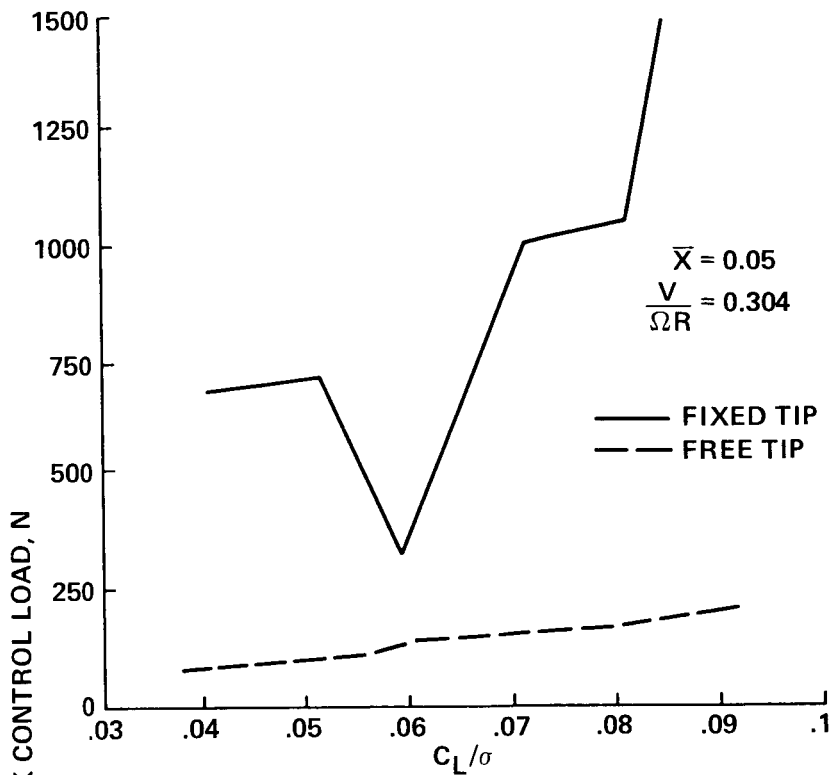



Figure 35.- Comparison of oscillatory loads going into the control system for the fixed- and free-tip configurations.

1. Report No. NASA TM-86751		2. Government Accession No.		3. Recipient's Catalog No.	
4. Title and Subtitle ANALYSIS OF THE FREE-TIP ROTOR WIND-TUNNEL TEST RESULTS				5. Report Date May 1985	
				6. Performing Organization Code	
7. Author(s) Robert H. Stroub				8. Performing Organization Report No. 85236	
9. Performing Organization Name and Address NASA Ames Research Center Moffett Field, CA 94035				10. Work Unit No.	
				11. Contract or Grant No.	
12. Sponsoring Agency Name and Address National Aeronautics and Space Administration Washington, D.C. 20546				13. Type of Report and Period Covered Technical Memorandum	
				14. Sponsoring Agency Code 505-42-11	
15. Supplementary Notes Point of Contact: Robert H. Stroub, Ames Research Center, MS 247-1, Moffett Field, CA 94035 (415) 694-6653 or FTS 464-6653					
16. Abstract <p>The results from a wind-tunnel test of a small-scale free-tip rotor are analyzed. The free-tip rotor has blade tips that are free to weathervane into the tip's relative wind, thus producing a more uniform lift around the azimuth. The free tip extended over the outer 10% of the rotor blade and included a simple, passive controller mechanism. The free-tip assembly, which includes the controller, functioned flawlessly throughout the test. In a test of the free-tip's response after passing through a vertical air jet, the tip pitched freely and in a controlled manner. Analysis of the tip's response characteristics showed the free-tip system's damped natural frequency to be 5.2 per rev. Tip pitch-angle responses to the local airstream are presented for an advance-ratio range of 0.1 to 0.397 and for a solidity weighted rotor lift-coefficient range of 0.038 to 0.092. Harmonic analysis of the responses showed a dominance by the first harmonic. Only at low advance ratios were there significant contributions from the higher harmonics. As a result of the tip being free, forward flight power requirements were reduced by 8% or more. Considerably more power reduction was recorded for high-thrust conditions. The reduction in power requirements was attributed to a favorable influence of the tip's negative pitch angle relative to the inboard portion of the blade; a hypothesis is presented to account for that favorable effect. The lessening of tip drag because of its negative relative pitch angle was also supported by fixed-wing wind-tunnel test of the same tip shape. In addition to the power reduction, flatwise blade bending moments were reduced by as much as 30% at the inboard blade stations. Chordwise loads, however, were not reduced by the free tip. Loads going into the control system were reduced at all speeds and rotor lift levels. Details of tip and controller design and construction are included.</p>					
17. Key Words (Suggested by Author(s)) Free tip Constant lift tip Blade tip Helicopter rotor Free-tip rotor Rotor tip shape			18. Distribution Statement  Subject Category: 05		
19. Security Classif. (of this report) Unclassified		20. Security Classif. (of this page) Unclassified		21. No. of Pages 69	22. Price*